BBA - Molecular Basis of Disease 1870 (2024) 166892

Contents lists available at ScienceDirect

BBA - Molecular Basis of Disease

journal homepage: www.elsevier.com/locate/bbadis

Local modulation of thyroid hormone signaling in the retina affects the development of diabetic retinopathy

Francesca Forini [a,1], Giuseppina Nicolini [a,1], Rosario Amato [b,1], Silvana Balzan [a], Alessandro Saba [c,f,g], Andrea Bertolini [c], Elena Andreucci [d], Silvia Marracci [b], Alberto Melecchi [b], Domiziana Terlizzi [a], Riccardo Zucchi [c], Giorgio Iervasi [e], Matteo Lulli [d,*], Giovanni Casini [b,f,g,**]

[a] Institute of Clinical Physiology, National Research Council, Pisa, Italy
[b] Department of Biology, University of Pisa, Pisa, Italy
[c] Department of Surgical, Medical and Molecular Pathology and Critical Care Medicine, University of Pisa, Pisa, Italy
[d] Department of Experimental and Clinical Biomedical Sciences "Mario Serio", University of Florence, Florence, Italy
[e] Department of Biomedical Sciences, National Research Council, Rome, Italy
[f] Interdepartmental Research Center Nutrafood "Nutraceuticals and Food for Health", University of Pisa, Pisa, Italy
[g] Center for Instrument Sharing (CISUP), University of Pisa, Pisa, Italy

ARTICLE INFO

Keywords:
Deiodinase enzymes
Low T3 state
miRNA
Mitochondrial dysfunction
Oxidative stress

ABSTRACT

Thyroid hormone (TH) dyshomeostasis is associated with poor prognosis in acute and prolonged illness, but its role in diabetic retinopathy (DR) has never been investigated. Here, we characterized the TH system in the retinas of db/db mice and highlighted regulatory processes in MIO-M1 cells. In the db/db retinas, typical functional traits and molecular signatures of DR were paralleled by a tissue-restricted reduction of TH levels. A local condition of low T3 (LT3S) was also demonstrated, which was likely to be induced by deiodinase 3 (DIO3) upregulation, and by decreased expression of DIO2 and of TH receptors. Concurrently, T3-responsive genes, including mitochondrial markers and microRNAs (*miR-133-3p*, *338-3p* and *29c-3p*), were downregulated. In MIO-M1 cells, a feedback regulatory circuit was evidenced whereby *miR-133-3p* triggered the post-transcriptional repression of *DIO3* in a T3-dependent manner, while high glucose (HG) led to DIO3 upregulation through a nuclear factor erythroid 2-related factor 2–hypoxia-inducible factor-1 pathway. Finally, an in vitro simulated condition of early LT3S and hyperglycemia correlated with reduced markers of both mitochondrial function and stress response, which was reverted by T3 replacement. Together, the data suggest that, in the early phases of DR, a DIO3-driven LT3S may be protective against retinal stress, while, in the chronic phase, it not only fails to limit HG-induced damage, but also increases cell vulnerability likely due to persistent mitochondrial dysfunction.

Abbreviations: ACF, acriflavine; ACN, acetonitrile; BRB, blood-retinal barrier; CPT2, carnitine palmitoyltransferase 2; DCFDA, 2′,7′-dichlorofluorescin diacetate; DIO2, type 2 deiodinase; DIO3, type 3 deiodinase; DMEM, Dulbecco's Modified Eagles Medium; DR, diabetic retinopathy; ERG, electroretinogram; FA, formic acid; FBS, fetal bovine serum; GFAP, glial fibrillary acidic protein; HIF-1, hypoxia inducible factor-1; HO-1, heme oxygenase-1; LC-MS/MS, liquid chromatography coupled with tandem mass spectrometry; LT3S, low T3 state; MeOH, methanol; MFN2, mitofusin 2; miRNA, microRNA; NF-kB, nuclear factor kappa-light-chain-enhancer of activated B cells; Nrf2, nuclear factor erythroid 2-related factor 2; OD, optical density; PB, phosphate buffer; PERG, pattern electroretinogram; PGC-1α, peroxisome proliferator-activated receptor-gamma coactivator-1α; phERG, photopic electroretinogram; phNR, photopic negative response; pNF-kB, nuclear factor kappa-light-chain-enhancer of activated B cells p65; qPCR, Real-Time PCR; RGC, retinal ganglion cells; ROS, reactive oxygen species; rT3, reverse triiodothyronine; scERG, scotopic electroretinogram; SPE, Solid Phase Extraction; T3, triiodothyronine; T4, thyroxine; TH, thyroid hormone; THRα, thyroid hormone receptor α; THRβ, thyroid hormone receptor β; VEGF, vascular endothelial growth factor; ZO1, zona occludens 1.

* Correspondence to: M. Lulli, Department of Experimental and Clinical Biomedical Sciences "Mario Serio", University of Florence, Viale Morgagni 50, 50134 Florence, Italy.

** Correspondence to: G. Casini, Department of Biology, University of Pisa, via San Zeno 31, 56127 Pisa, Italy.

E-mail addresses: francesca.forini@cnr.it (F. Forini), giuseppina.nicolini@cnr.it (G. Nicolini), rosario.amato@unipi.it (R. Amato), alessandro.saba@unipi.it (A. Saba), a.bertolini2@student.unisi.it (A. Bertolini), e.andreucci@unifi.it (E. Andreucci), silvia.marracci@unipi.it (S. Marracci), a.melecchi@student.unisi.it (A. Melecchi), riccardo.zucchi@unipi.it (R. Zucchi), giorgio.iervasi@cnr.it (G. Iervasi), matteo.lulli@unifi.it (M. Lulli), giovanni.casini@unipi.it (G. Casini).

[1] Authors contributed equally to this work.

https://doi.org/10.1016/j.bbadis.2023.166892
Received 25 July 2023; Received in revised form 5 September 2023; Accepted 19 September 2023
Available online 25 September 2023

1. Introduction

Neuronal damage has increasingly emerged as a primary pathophysiologic trait of diabetic retinopathy (DR) [1–3], and protective mechanisms are elicited in the retina in order to protect the neurons. For instance, the upregulation of vascular endothelial growth factor (VEGF), classically considered as a pathological hallmark in advanced stages of DR, is likely to be induced as an early neuroprotective strategy [4,5]. Similarly, the early activation of autophagy may represent a retinal response to contrast high glucose (HG)-induced cell death by apoptosis [6]. Reduction of cell metabolism and of energy expenditure may represent another mechanism by which the retina, similar to other tissues, tries to protect itself from stress. Thyroid hormones (THs), namely the biologically active 3,5,3′-triiodothyronine (T3) and its precursor thyroxine (T4), are well known regulators of metabolic homeostasis via activation of mitochondrial biogenesis, respiration, function, and quality control [7–9]. Therefore, decreasing the intraretinal levels of THs may represent a retinal strategy, similar to those involving VEGF overexpression or autophagy activation, to reduce oxidative stress and cell damage under hyperglycemic condition. Even though this compelling hypothesis has never been investigated, the presence of TH receptors [10–12], of the monocarboxylate transporter 8 [13], of TH responsive cells [14], and of deiodinase enzymes [15,16] in the retina suggests the possibility of a retinal, local regulation of the TH system to reduce retinal stress. For instance, anti-TH treatments in experimental models of congenital retinal diseases have been observed to protect cone photoreceptors from degeneration [17–19]. However, a prolonged reduction of T3 levels, known as low T3 state (LT3S) might turn disadvantageous when critical illness enters a chronic phase [20–23]. Indeed, subclinical hypothyroidism has been found to be associated with DR in diabetic patients [24], and reduced T3 and T4 serum levels, even in the euthyroid range, have been described to be negatively correlated with DR in type 2 diabetic patients [25,26]. Generally, LT3S is associated with disease progression and poor long-term prognosis [20–23,27]. In these cases, adverse conditions might be mitigated by re-establishment of T3 physiological levels, as observed in a rat model of cardiac ischemia and reperfusion and in patients with myocardial infarction [28–31]. Noteworthy, in addition to systemic alterations of TH levels, local derangements of TH signaling can be observed in several physiopathological conditions independent of T3 and T4 serum concentrations [32–35]. The main processes contributing to the regional lowering of TH bioavailability in different diseased tissues and organs are likely to include decreased TH cellular uptake, along with inhibition of type 2 deiodinase 2 (DIO2), the enzyme responsible for the activation of T4 into T3, and upregulation of type 3 deiodinase (DIO3), a fetal protein which converts T4 into the biologically inactive reverse T3 (rT3) [36].

It is still unknown whether, similar to other pathological conditions, an intraretinal TH dyshomeostasis may be the result of an increased activity or expression of *DIO3* or a reduction of *DIO2*. Our hypothesis is that in the retina, as in other organs or tissues, a LT3S develops as an adaptive response to protect against diabetes-induced stressful conditions, and that it may turn detrimental in the chronic stage contributing to the progression of retinal damage.

Regarding possible mechanisms by which TH signaling may impact on the retina in DR, an intriguing hypothesis is that LT3S may affect recently identified T3-dependent microRNA (miRNA)/gene regulatory circuits [30]. For instance, in a model of acute myocardial infarction in rats, the downregulation of *miR-133*, *miR-338*, and *miR-29*, which are also likely to be involved in DR evolution, was rescued by T3 replacement [30]. Also, miRNA expression is altered in DR [37–39] and some of the involved miRNAs may be associated with the regulation of retinal TH. If, on the one hand, retinal TH signaling may depend on miRNA-regulated mechanisms, on the other the modulation of T3 levels is likely to affect the retina through altered mitochondrial function. Since mitochondria play a significant role in the development of DR [40], it is plausible that TH dyshomeostasis may contribute to the pathophysiology of the disease by interfering with mitochondrial activity.

The aims of the present work were (1) to demonstrate the presence of a LT3S in the retina of db/db mice (a model of type 2 diabetes) in concomitance with the presence of typical markers of DR; (2) to investigate, in an in vitro model, the possibility of a miRNA-based mechanism for the regulation of retinal T3 levels; (3) to get insights into the possible involvement of a LT3S -induced mitochondrial deregulation in the development of DR.

2. Materials and methods

2.1. Animals

BKS.Cg-+Lepr^{db}/+Lepr^{db}/OlaHsd (db/db) male mice (ENVIGO, San Pietro al Natisone, Udine, Italy), which are affected by type 2 diabetes [41–43], were used. C57BL/6J mice were used as controls. In respect of the 3Rs principles for ethical use of animals in scientific research, the retinas analyzed in these studies derived from animals (both db/db and controls) also used for a study on dermal tissue regeneration without any involvement of the retinas or any other ocular tissues [44]. All the procedures were performed in compliance with the ARVO Statement for the Use of Animals in Ophthalmic and Vision Research, the EU Directive (2010/63/EU), and the Italian guidelines for animal care (DL 26/14; Italian Ministry of Health, decree numbers 905/2018-PR and 132/2019-PR). At the moment of analysis, the mice were sixteen-week-old. Non-fasting glycemia was measured by tail sampling using a OneTouch Ultra glucometer (LifeScan Inc., Milpitas, CA, USA). A total of 34 db/db and 15 control mice were used in these studies.

2.2. Electroretinography

The mice were subjected to an electroretinogram (ERG) recording routine that included an analysis of the rod pathway with scotopic ERG (scERG), an analysis of the cone pathway with photopic ERG (phERG), and an analysis of retinal ganglion cell (RGC) activity with pattern ERG (PERG). After overnight dark-adaption, the mice were anesthetized by an intraperitoneal injection of Avertin (1.25 % avertin/g body weight) and gently restrained in a custom-made stereotaxic apparatus allowing an unobstructed visual field. Body temperature was maintained at 37 °C by mean of a feedback-controlled heating pad and corneal moisture was ensured by adding balanced saline solution before and during the recording session. Recording electrodes, consisting in a loop-shaped silver-silver chloride wire, were carefully laid on the corneal surface of each eye using micro manipulators. Stainless steel needles, one for each eye, were used as reference electrodes after being inserted subcutaneously on the mouse scalp, while an additional stainless steel needle was inserted at the tail root and used as ground electrode. ERG responses were recorded and analyzed using a commercially available ERG setup (Retimax Advanced, CSO, Firenze, Italy). ERG routine for each mouse provided the sequential recording of scERG, phERG and PERG. scERG recordings were performed by delivering five consecutive flash stimuli at 10 cd·s/m^2 by means of a Ganzfeld bowl. Signals recorded simultaneously from each eye were averaged to reduce noise after 5000-fold amplification and 1–100 Hz band-pass filtering. The average scERG waveforms were analyzed by measuring the amplitude of the a-wave (baseline to trough) and that of the b-wave (trough to peak). Immediately after the scERG session, the mice were adapted to 40.0 cd·s/m^2 rod-saturating light for 1 min. Thence, cone-driven phERG responses were recorded by delivering 50 consecutive flashlight stimuli at 5 cd·s/m^2 over the same adaptation background. The phERG responses simultaneously recorded from both eyes were amplified (5000-fold) and band-pass filtered (1–100 Hz). The average phERG responses were calculated by measuring the b-wave amplitude (baseline to peak) and the photopic negative response (PhNR) amplitude (baseline to trough). Finally, PERG recordings were acquired by delivering a visual stimulus

consisting of contrast-reversing black and white (98 % contrast; 1 Hz temporal frequency) by means of a 19″ light emitting diode display (area: 74° × 62°) aligned to the mouse cornea and spaced 25 cm from the mouse eye (0.05 cyc/deg spatial frequency). PERG signals deriving from each pattern reversal were amplified (10000-fold) and band-pass filtered (1–30 Hz). Overall, the responses deriving from 900 consecutive pattern reversals were averaged to reduce noise contamination by a factor of $\sqrt{900} = 30$. The average PERG responses were calculated by detecting the early positive inflection point (N35), the positive peak (P50) and the belated negative trough (N95) to measure N35-P50 and P50-N95 amplitudes. Immediately after ERG routine, mice were euthanized by cervical dislocation, retinas were collected, immediately frozen in liquid nitrogen, and stored at −80 °C until assay.

2.3. Immunofluorescence

Glial activation was assessed with an evaluation of glial fibrillary acidic protein (GFAP) immunofluorescence in Müller cells. This process, called reactive gliosis, is typical of certain chronic pathologies, such as DR [45]. Both control and db/db mice were sacrificed by cervical dislocation. Their eyes were dissected and immersion fixed for 2 h at room temperature in 4 % paraformaldehyde in 0.1 M phosphate buffer (PB) and then stored at 4 °C in 25 % sucrose in 0.1 M PB. Subsequently, the eyes were embedded in cryo-gel, frozen using liquid nitrogen, and cut into 10 μm thick coronal sections with a cryostat. The sections were mounted onto gelatinized slides and stored at −20 °C until use. For immunostaining, the sections were incubated overnight with a rabbit monoclonal antibody directed to GFAP (ab207165, dilution 1:400; Abcam, Cambridge, United Kingdom) in PB containing 5 % bovine serum albumin and 2 % TritonX-100. After overnight incubation, the sections were incubated with secondary antibody conjugated with Alexa-Fluor-488 (Life Technologies, Carlsbad, CA, USA, 1:200 dilution) at room temperature for 2 h. Finally, the slides were coverslipped with Fluoroshield Mounting Medium containing DAPI (Abcam). The images were acquired using an epifluorescence microscope (Nikon Europe, Amsterdam, The Netherlands) and adjusted for contrast and brightness using Adobe Photoshop (Adobe Photoshop CS3; Adobe Systems, Mountain View, CA, USA).

2.4. Liquid chromatography coupled with tandem mass spectrometry (LC-MS/MS)

Materials and chemicals: T3, $^{13}C_6$-T3, T4, and $^{13}C_6$-T4 solutions, 100 μg/mL in methanol (MeOH) with 0.1 M NH_3, were purchased from Sigma Aldrich-Merck (St. Louis, MO, USA), as well as water LC-MS grade, MeOH LC-MS grade, acetonitrile (ACN) LC-MS grade, 2-propanol LC-MS grade, hexane HPLC grade, dichloromethane HPLC grade, ammonium hydroxide (28 % NH_3 in H_2O, ≥99.99 % trace metal basis), formic acid LC-MS grade (FA, ≥98 %). Bond-Elut Certify 130 mg Solid Phase Extraction (SPE) cartridges were obtained from Agilent Technologies (Santa Clara, CA, USA), while homogenizing 2 mL Precellys tubes were purchased from Bertin Technologies (Montigny-le-Bretonneux, France).

2.4.1. Sample preparation (retinas)

Frozen retinas were quickly transferred to 2 mL homogenizing Precellys tubes, weighted and processed as reported previously [46,47]. Each sample was suspended in 1 mL of a solution made of 840 μL of ACN and 150 μL of pure water added with 10 μL of a 10 ng/mL internal standard mixture ($^{13}C_6$-T3 and $^{13}C_6$-T4). After being vortexed, samples were sonicated for 15 min and then homogenized using a Precellys 24-Dual Homogenizer (Bertin Technologies) through three homogenization steps of 45 s with 60 s pause at 5000 rpm. Homogenized samples were sonicated again for 15 min and then centrifuged for 15 min at 22780 ×*g*. Supernatants were transferred to new 2 mL Eppendorf tubes and washed three times using 1 mL of hexane to remove the phospholipid excess. The lower phase was dried under a gentle stream of nitrogen in a thermostated block at 40 °C. The samples were reconstituted using 100 μL of H_2O: MeOH 70:30 (v/v), vortexed for 10 min, centrifuged for 15 min at 22780 ×*g*, and 20 μL were injected in the LC-MS/MS system. The quantification of analytes was performed using standard T3 and T4 calibration curves built in methanol from 0.025 ng/mL to 5 ng/mL.

2.4.2. Sample preparation (serum)

Serum samples, collected from the mice at the time of sacrifice, were processed as previously reported [46,48]. Briefly, 100 μL serum were added with 10 μL of a 200 ng/mL internal standard mixture ($^{13}C_6$-T3 and $^{13}C_6$-T4), equilibrated for 30 min at room temperature, then 300 μL of cold acetone were added and samples were vortexed and kept 30 min at 4 °C to allow protein precipitation. After centrifugation at 22780 ×*g* for 10 min, the supernatants were dried in a thermostated block at 40 °C under a nitrogen stream until reaching ~100 μL. Afterwards, samples were added with 400 μL of a 0.1 M potassium acetate buffer (pH = 4) and submitted to SPE using Agilent Bond-Elut Certify 130 mg SPE cartridges. Before samples loading, cartridges were conditioned by consecutive wetting with 2 mL of dichloromethane/2-propanol (75/25 v/v), 2 mL of methanol and 2 mL of 0,1 M potassium acetate buffer (pH = 4). After four consecutive washing steps using 3.5 mL of water, 2 mL of 0.1 M hydrochloric acid, 7 mL of methanol and 3.5 mL of dichloromethane/2-propanol (75/25 v/v), samples were eluted with 2 mL of dichloromethane/2-propanol/ammonium hydroxide (70/26.5/3.5 v/v/v). Eluates, warmed up at 40 °C, were dried, reconstituted with 100 μL of MeOH/H_2O (30/70, v/v) and 5 μL were injected into the LC-MS/MS system. Calibration curves were prepared by serial dilution with methanol at concentrations ranging from 0.10 to 100 ng/mL.

2.4.3. LC-MS/MS instrumental layout

The instrumental layout consisted in an Agilent (Santa Clara, CA, USA) 1290 UHPLC system, including a binary pump, a column oven set at 20 °C and a thermostated autosampler, coupled to an AB-Sciex (Concord, Ontario, Canada) QTRAP 6500+ mass spectrometer working as a triple quadrupole, equipped with an IonDrive™ Turbo V source. Chromatographic separation was achieved by using a 110 Å, 2 × 50 mm, 3 μm particle size, Gemini C18 column (Phenomenex, Torrance, CA), protected by a C18 Security Guard Cartridge and using (A) MeOH/ACN (20/80 by volume) added with 0.1 % FA and (B) water containing 0.1 % FA as mobile phases. The integrated switching valve was used to discard both head and tail of the HPLC runs. Gradient elution (400 μL/min flow rate) was performed as follows: 0.1–3 min (A) 5 %, 8.5 min (A) 65 %, 9.0–11.0 min (A) 100 %, 11.50–13.50 (A) 5 %. System control, data acquisition and analyses were performed using an AB Sciex Analyst® version 1.7 software. More details are given in Table S1 and Supplementary Methods.

2.5. MIO-M1 cell culture

In vitro studies were performed using MIO-M1 cells, kindly provided by Dr. Gloria Astrid Limb (Division of Ocular Biology and Therapeutics, UCL Institute of Ophthalmology, London, UK). MIO-M1 is a spontaneously immortalized human Müller cell line, which retains morphologic features, marker expression and electrophysiological responses of primary isolated Müller cells in culture. MIO-M1 cells were cultured in Dulbecco's Modified Eagles Medium (DMEM, Lonza, Basel, Switzerland) containing 5.5, or 25.0 mM glucose supplemented with 10 % fetal bovine serum (FBS), 100 U/mL Penicillin-Streptomycin, and 2 mM L-Glutamine (Euroclone, Milano, Italy) in a humidified incubator at 37 °C in 5 % CO_2. The experiments were performed at 60–80 % cell density. In the experiments involving T3 treatment, FBS was substituted with the same amount of FBS deprived of TH with standard charcoal stripping procedures (TH-free medium), in line with previous studies [49] and with the American Thyroid Association guidelines [50]. Briefly, FBS was absorbed overnight at 4 °C on dextran-coated activated charcoal (40

mg/mL serum), the suspension was centrifuged to precipitate the charcoal and the supernatant was filtered through 0.2 μm filters. The culture medium was changed every other day. In different experiments, MIO-M1 cells were treated with T3 at physiological concentrations (3 nM), 5 μM K67 (a Nuclear factor erythroid 2-related factor 2 [Nrf2] inhibitor), or 5 μM acriflavine (ACF, a hypoxia inducible factor-1 [HIF-1] inhibitor).

2.6. RNA extraction, cDNA synthesis, and Real-Time PCR (qPCR)

Total RNA from retinal samples or MIO-M1 cell cultures was extracted with the miRNeasy mini kit reagent (Qiagen, Hilden, Germany) or TRI reagent (Sigma-Aldrich) according to the manufacturer's instructions. The cDNA was synthesized from 500 ng RNA using the QuantiTect Reverse Transcription Kit (Qiagen, Hilden, Germany) and the LunaScript®RT SuperMix Kit (New England BioLabs) (for mRNA transcript analysis), or the miScript II RT kit (Qiagen, Hilden, Germany) (for miRNA transcript analysis) as indicated by the manufacturers.

For gene and miRNA expression analyses, the cDNA was processed in triplicate in a Rotor-Gene Q real-time machine (Qiagen, Hilden, Germany) using the Quantifast SYBR Green Mix (Qiagen, Hilden, Germany) and the Luna®Universal qPCR Master Mix (New England BioLabs) (for mRNA transcript analysis). To assess product specificity, a melting curve analysis from 65 °C to 95 °C with a heating rate of 0.1 °C/s with a continuous fluorescence acquisition was constructed. Gene transcript values were normalized using *Hprt*, *Hmbs* or beta2 microglobulin (*B2M*) reference genes. miRNA transcript values were normalized using *SnRNA-U6* and *SnRNA-U1*. The relative quantification of samples was performed by Rotor Gene Q-Series Software (Qiagen, Hilden, Germany). The analyzed miRNAs included *miR-133a-3p*, *miR-338-3p*, and *miR-29c-3p* (from now on indicated as *miR-133a*, *miR-338* and *miR-29c*, respectively). The complete list of primer sequences is shown in Table S2A and B.

2.7. Western blotting

For Western blot assay, retinal samples or MIO-M1 cell cultures were lysed by three sonication cycles in RIPA lysis buffer (Santa Cruz Biotechnology, Dallas, TX, USA) supplemented with phosphatase and proteinase inhibitor cocktails (Roche Applied Science, Indianapolis, IN, USA). The protein content was quantified by using Micro BCA Protein Assay (Thermo Fisher Scientific, Waltham, MA, USA). Thirty micrograms of protein of each sample were separated by SDS-PAGE (4–20 %; Bio-Rad Laboratories, Inc., Hercules, CA, USA) and transferred onto nitrocellulose membranes (Bio-Rad). Membranes were blocked with 5 % non-fat diet milk for 1 h at room temperature, and subsequently incubated overnight at 4 °C with the primary antibody (Table S3). After washing in 1× Tris-Buffered Saline containing 0.05 % Tween-20, membranes were incubated for 1 h at room temperature with HRP-conjugated secondary anti-mouse or anti-rabbit antibodies (Table S3). Blots were developed by the Clarity western enhanced chemiluminescence substrate (Bio-Rad), and the signal was detected by means of ChemiDoc XRS+ (Bio-Rad). The optical density (OD) of the target bands was evaluated by ImageLab 3.0 software (Bio-Rad). The data were normalized to the corresponding OD of β-actin or of nuclear factor kappa-light-chain-enhancer of activated B cells (NF-kB), as appropriate loading control.

2.8. In silico analysis

The interaction between the 3′UTR of human, rat, and mouse *DIO3* transcripts and the seed sequence of the conserved *miR-133a* was predicted in a previous paper [51]. The interactions between the 3′UTR of human, rat, and mouse *DIO3* transcripts and the seed sequence of the conserved *miR-338* or *miR-29c* were predicted using the online miRNA target prediction tools miRWalk and TargetScan available at the following links: http://mirwalk.umm.uni-heidelberg.de/; https://www.targetscan.org/vert_80 (accessed on September 22, 2022).

2.9. Luciferase activity assay

The dual firefly-and-renilla/luciferase-reporter gene assay was performed to evaluate the ability of *miR-133a* and *miR-338* to directly bind the 3′ untranslated regions (3′UTR) of *DIO3* mRNA and repress translation. The reporter vector was generated by cloning the entire sequence of the mouse *DIO3* 3′UTR transcript downstream the luciferase reporter gene within the pGLU Dual-luciferase reporter plasmid vector as previously described [43]. For the luciferase assays, MIO-M1 cells were plated in 12-multiwell plates at a density of approximately 80,000 cells per well and maintained in DMEM with 5.5 mM glucose. After plating for 24 h, the cells were cotransfected via 6 h incubation with 500 ng of reporter vector, 100 ng of pRL control vector-TK (Renilla, Promega, Madison, WI, USA), and increasing concentrations of the *miR-133a* or *miR-338* mimic (0.25 nM, 50 nM, 100 nM). The control mimic was used to ensure an equal total concentration of miR mimic in each well. As transfectant, 1.5 μL aliquots of lipofectamine 2000/well (Thermo Fisher Scientific) were used according to the manufacturer's instructions. After transfection for 48 h, the cells were processed with the Dual-Luciferase Reporter Assay System (Promega) kit according to the manufacturer's instructions. Briefly, after cell lysis and recovery of the cytosolic fraction by 10 min centrifugation at 12,000 rpm, the luminescence was quantified in 20 μL of the sample using the GloMax-Multi detection system (Promega) luminometer.

2.10. miRNA gain and loss of function

For *miR-133a* and *miR-338* gain and loss of function experiments, MIO-M1 cells were plated in 12-multiwell plates at a density of approximately 80,000 cells per well and maintained in TH-free medium with 5.5 mM glucose. After plating for 24 h, the cells were transfected for 5 h with a mixture containing 1.5 μL of transfectant lipofectamine 2000 (Thermo Fisher Scientific) and 100 nM of the *miR-133a* mimic or control mimic (Eurofins Genomics, Ebersberg, Germany), or 2′*O*-methylated-*mir133a* decoy or control 2′*O*-methylated decoy (Eurofins Genomics). The mimic and decoy sequences are shown in Table S4. At the end of the transfection protocol, the cells were kept for 48 h in TH-free medium with 5.5 mM glucose in the presence or absence of 3 nM T3 and then evaluated for *DIO3* mRNA expression with qPCR.

2.11. Evaluation of intracellular ROS levels by flow cytometry

Reactive oxygen species (ROS) were evaluated in MIO-M1 cells cultured with 5.5 or 25 mM glucose for 24 h. Subsequently, the cells were detached using trypsin-EDTA (Euroclone, Milan, Italy), centrifuged at 400 ×*g* for 5 min and then re-suspended in complete medium that was pre-equilibrated at 37 °C with 5 μM of DCFDA (Sigma-Aldrich). The cells were then incubated for 30 min at 37 °C, in the dark. A positive control sample was prepared adding 20 mM H_2O_2 during the incubation with the dye. The cells were then promptly analyzed through a BD FACSCanto II Flow Cytometer detecting DCFDA fluorescence in the FITC channel and the results were analyzed using the FlowJo software.

2.12. Statistical analysis

All variables met the condition for parametric analysis. Data were analyzed using either Student's *t*-test, for single comparisons, or one-way analysis of variance (ANOVA) followed by Tukey's post-hoc test, for multiple comparisons. The results were expressed as mean ± SEM of the biological replicates in each experiment (individual data points are shown in each graph; Prism 8; GraphPad software, San Diego, CA, USA). Differences with $p < 0.05$ were considered significant.

3. Results

3.1. Glycemia and plasma levels of T3 and T4 in db/db mice

As expected, db/db mice displayed a significantly increased blood glucose concentration, with respect to controls, with values around 500 mg/ml (Fig. 1A). This alteration of glycemia did not correlate with changes of circulating TH levels. Indeed, neither T3 (Fig. 1B) nor T4 (Fig. 1C) plasma levels were altered in db/db mice.

3.2. The retinas of db/db mice display functional traits and molecular signatures typical of DR

The electroretinographic routine displayed in Fig. 2 was designed to obtain a comprehensive evaluation of the retinal function, including dark- and light-adapted activity of photoreceptors, post-receptoral retina and RGCs. The analysis of the dark-adapted scERG (Fig. 2A) revealed a significant decrement, in db/db mice as compared to controls, of both the photoreceptor-related a-wave amplitude and the b-wave amplitude, related to dark-adapted post-receptoral activity.. In addition to alterations in the dark-adapted response, mainly deriving from the rod pathway, db/db mice also displayed altered light-adapted phERG responses relative to cone-mediated retinal activity (Fig. 2B). In this respect, db/db mice displayed a significant decrease in the amplitudes of both post-receptoral phERG b-wave and the RGC-related PhNR as compared with those of control mice. The overall alteration in receptoral and post-receptoral activity in db/db mice was reflected on impaired RGC activity, specifically assessed using PERG (Fig. 2C). In this respect, db/db mice displayed significant alterations of both the n35-p50 and p50-n95 components of the response as compared to controls.

Together with retinal functional alterations, a different pattern of GFAP immunofluorescence was observed between control and db/db retinas. As shown in Fig. 2D, GFAP immunofluorescence in controls was confined to astrocytes within the ganglion cell layer, while in retinas of db/db mice it labeled the processes of numerous Müller cells typically extending throughout the retinal thickness (Fig. 2E).

The retinal levels of Nrf2 and NF-kB were investigated as major markers of oxidative stress and inflammation, respectively. In particular, Nrf2 is a redox-sensitive transcription factor that, in response to increased free radicals, enters the cell nucleus and promotes the transcription of antioxidant genes [52]. On its hand, NF-kB is an oxidant-sensitive transcription factor that regulates the expression of genes involved in inflammatory responses [53], and the levels of its phosphorylated form pNF-kB can be used as an index of pro-inflammatory activity. As shown in Fig. 2F, Nrf2 protein levels were significantly increased in the retinas of db/db mice with respect to controls, indicating the presence of high levels of oxidative stress. At the same time, the retinas of db/db mice showed a pNF-kB/NF-kB ratio higher than that in control retinas (Fig. 2G), indicating an increased pro-inflammatory activity. Increased levels of oxidative stress and inflammatory markers in db/db retinas were associated with typical hallmarks of DR such as VEGF overproduction and damage of the blood-retinal barrier (BRB). In this respect, qPCR data showed that db/db retinas had significantly higher expression of *VEGF* mRNA (Fig. 2H) and lower expression of zona occludens 1 (*ZO1*, a protein of the tight junction expressed in the BRB) mRNA than control retinas (Fig. 2I).

3.3. Diabetes induces significant changes in TH levels and in markers of TH signaling in the retina

TH concentrations measured in the retina using mass spectrometry showed that both T3 and T4 levels were significantly reduced with respect to those in control retinas: T3 3.04 ± 0.39 pmol/g vs 4.43 ± 0.52 pmol/g (Fig. 3A); and T4, 2.88 ± 0.30 vs 11.45 ± 1.18 pmol/g (Fig. 3B).

The marked changes in T3 and T4 concentrations observed in db/db retinas were likely to be caused by changes in *DIO2* and *DIO3* expression. The relative qPCR analysis showed that, with respect to controls, in db/db retinas *DIO2* mRNA expression was dramatically reduced (Fig. 3C), while *DIO3* mRNA expression was increased significantly (Fig. 3D). Consequently, the ratio *DIO3/DIO2* mRNA was also increased (Fig. 3E). At the level of protein content, DIO2 was significantly decreased in db/db with respect to control retinas, although to a much lower extent than *DIO2* mRNA (Fig. 3F), while both DIO3 protein (Fig. 3G) and the DIO3/DIO2 protein ratio (Fig. 3H) were significantly increased.

The most prevalent TH receptors in the adult murine central nervous system are THRα1 (60 % of the total) and THRβ2 (30 % of the total) [54]. As shown in Fig. 4, the expression of both receptor types was significantly decreased in db/db compared to control retinas, both at the mRNA (Fig. 4A, B) and at the protein (Fig. 4D, E) level, but the ratios *THRα1/THRβ2* mRNA (Fig. 4C) and THRα1/THRβ2 protein (Fig. 4F) were not significantly different between control and db/db retinas.

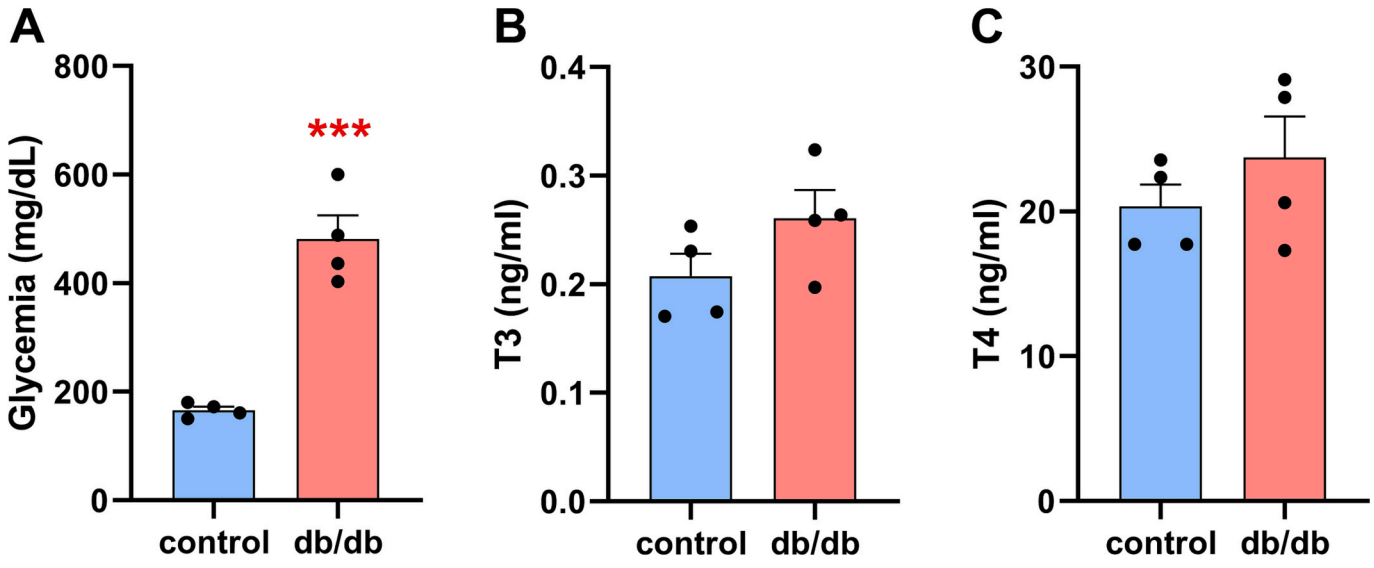

Fig. 1. Blood glucose levels (A) and plasma concentrations of T3 (B) and of T4 (C) evaluated with mass spectrometry in db/db mice at 16 weeks of age compared to co-aged wild type mice (control). ***$p < 0.001$ vs. control.

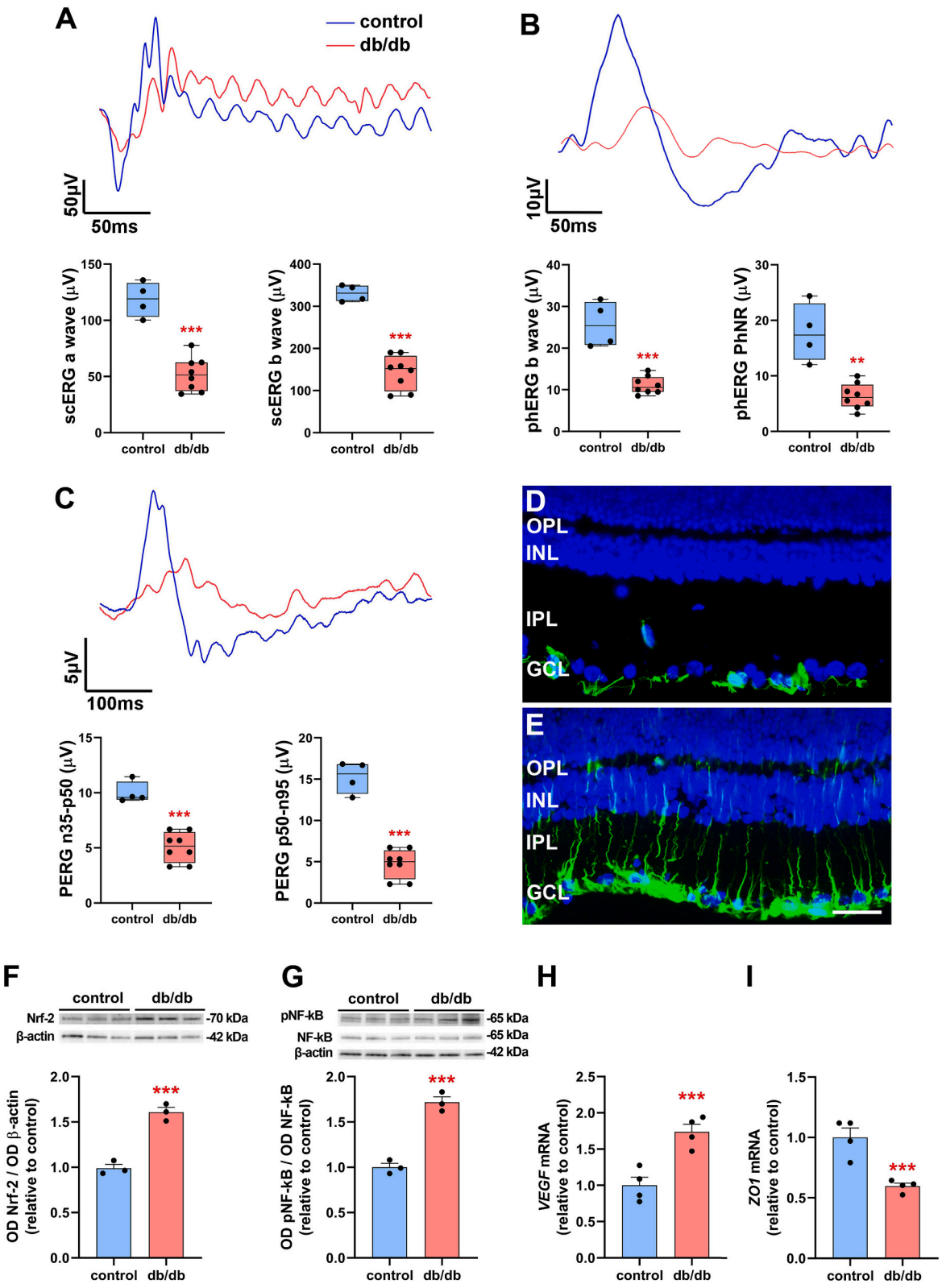

Fig. 2. Analysis of variations in retinal activity and in markers of DR in retinas of db/db mice at 16 weeks of age compared to co-aged wild type mice (control). (A) Representative recordings and quantitative analysis of scERG responses. Statistically significant reductions were observed in the db/db retinas relative to the amplitudes of both the a-wave and the b-wave. (B) Representative recordings and quantitative analysis of phERG responses. Statistically significant reductions were observed in the db/db retinas relative to the phERG b-wave amplitude and to the PhNR amplitude. (C) Representative recordings and quantitative analysis of PERG responses. db/db mice showed a significant reduction of the response in both the n35-p50 and the p50-n95 components. (D) and (E) show the GFAP immunostaining patterns in control and db/db retinas, respectively (scale bar, 50 μm). (F) and (G) show the immunoreactive bands and the protein levels, relative to control, of Nrf2 and of pNF-kB/NF-kB, respectively. β-Actin was used as an internal standard. (H) and (I) show the mRNA levels, relative to control, of *VEGF* and of *zona occludens 1* (*ZO1*) mRNA, respectively. GCL, ganglion cell layer; INL, inner nuclear layer; IPL, inner plexiform layer; OPL, outer plexiform layer. **p < 0.01, ***p < 0.001 vs control.

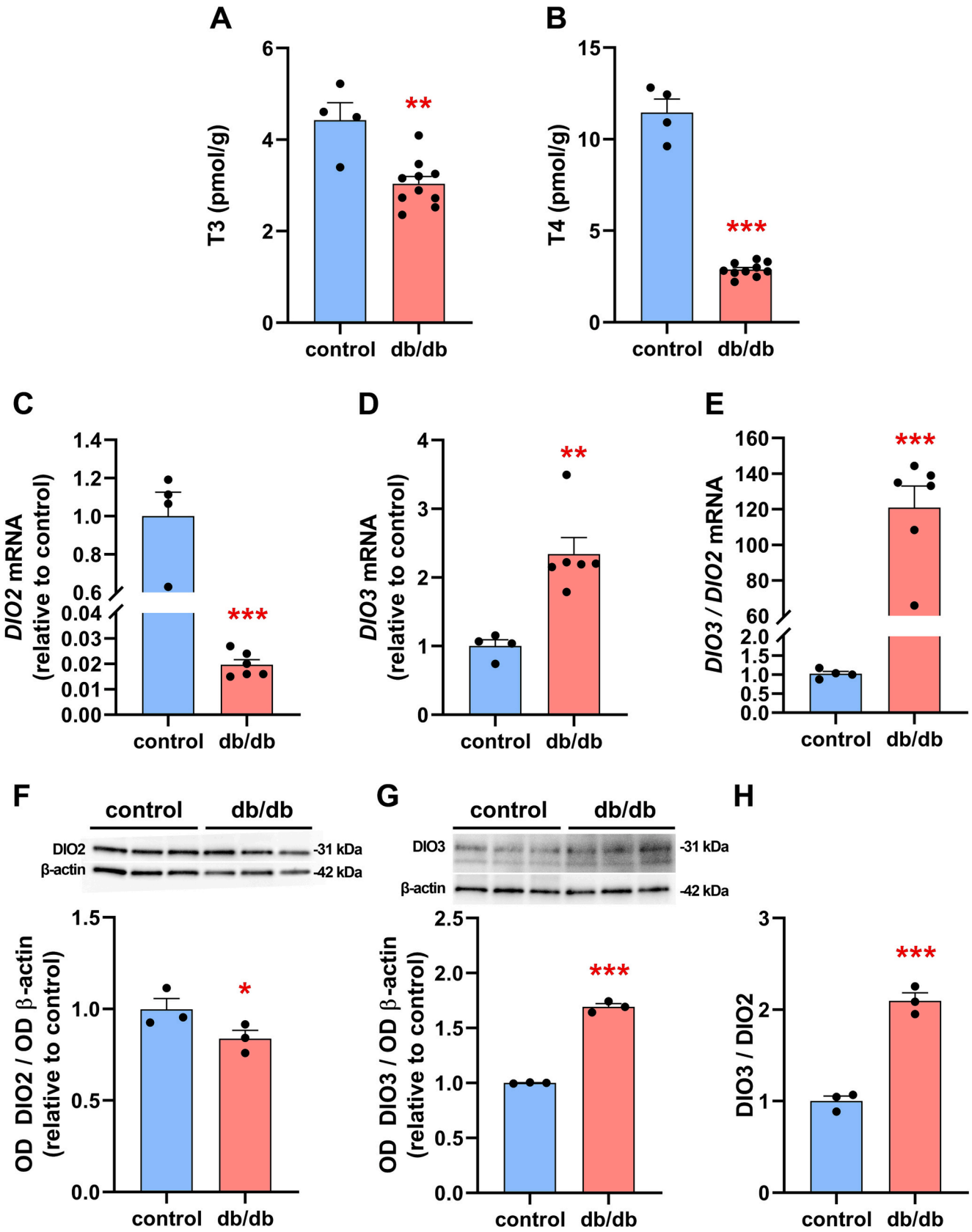

Fig. 3. TH levels and deiodinase enzyme expression in retinas of db/db mice at 16 weeks of age compared to co-aged wild type mice (control). (A) and (B) show, respectively, T3 and T4 levels evaluated with mass spectrometry. *DIO2* and *DIO3* mRNA expression levels are shown in (C) and (D), respectively, while the ratio *DIO3/DIO2* mRNA is shown in (E). Western blots showing immunoreactive bands and protein levels of DIO2 and DIO3 are in (F) and (G), respectively, while the ratio DIO3/DIO2 protein is shown in (H). *$p < 0.05$, **$p < 0.01$, ***$p < 0.001$ vs control.

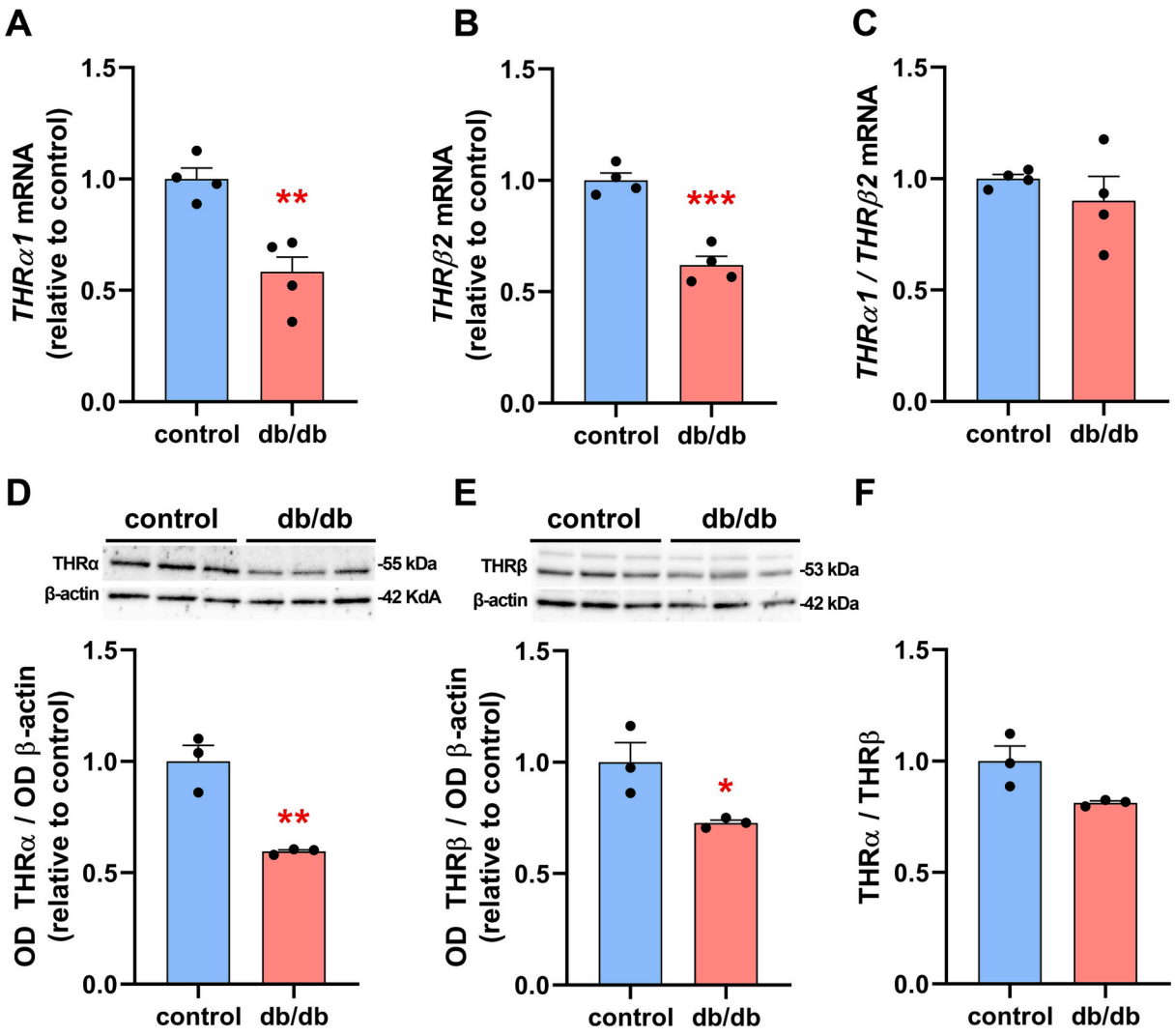

Fig. 4. THR expression in retinas of db/db mice at 16 weeks of age compared to co-aged wild type mice (control). *THRα1* mRNA and *THRβ2* mRNA levels are shown in (A) and (B), respectively, while the ratio *THRα1/THRβ2* mRNA is shown in (C). Western blots (immunoreactive bands and protein levels) of THRα and THRβ are in (D) and (E), respectively, while the ratio THRα/THRβ protein is shown in (F). *p < 0.05, **p < 0.01, ***p < 0.001 vs control.

3.4. Expression of T3-responsive miRNAs and markers of mitochondrial function are altered in db/db retinas

Given the pivotal role of T3-dependent miRNAs in fine tuning TH action, we investigated the retinal expression of *miR-133a*, *miR-338*, and *miR-29c*, three miRNAs that have been previously observed to be downregulated by stress (cardiac ischemia) and upregulated by T3 replacement [31]. As shown in Fig. 5A–C, all the three miRNAs were markedly downregulated in the retinas of db/db mice with respect to controls. Regarding the analysis of TH-responsive markers of mitochondrial function, peroxisome proliferator-activated receptor-gamma coactivator 1 alpha (PGC-1α) is known as the master regulator of mitochondrial biogenesis and metabolic homeostasis [55], carnitine palmitoyltransferase 2 (CPT2) is an enzyme essential for β oxidation of long-chain fatty acids in the mitochondria [56], and mitofusin 2 (MFN2) is an outer mitochondrial membrane GTPase playing critical roles in mitochondrial dynamic and quality control, together with MFN1 and protein OPA1, [57]. As shown in Fig. 5D–F, the transcripts of *PGC-1α*, *CPT2*, and *MFN2* were significantly reduced in db/db retinas as compared to controls.

3.5. MIO-M1 cells respond to HG with modulation of deiodinase enzyme expression in a Nrf2/HIF-1α-dependent manner

To investigate possible mechanisms involving TH signaling in both the healthy and the diseased retina, in vitro studies were designed using MIO-M1 cells as experimental models. As a first step, to corroborate the in vivo results, we sought to confirm the causal involvement of HG exposure in the induction of a stress response and in the modulation of DIO enzymes. To this purpose, we evaluated the levels of oxidative stress and of *VEGF* expression along with the expression of *DIO2* and *DIO3* in cells exposed to HG. Not surprisingly, MIO-M1 cells responded to a 24 h HG treatment with increased ROS production (Fig. 6A, B) and *VEGF* upregulation (Fig. 6C). In addition, in line with the in vivo study, both 24 and 72 h of incubation in HG resulted in significant downregulation of *DIO2* paralleled by upregulation of *DIO3* both at level of gene expression and protein content (Fig. S1, Fig. 6D and E).

Regarding possible mechanisms of *DIO3* induction under stress conditions, evidence in extra-retinal tissues demonstrates that *DIO3* may be upregulated through a HIF-1α-dependent pathway [58]. In addition, a variety of experimental observations indicate that oxidative stress may stimulate HIF-1α stabilization through Nrf2 activation and, likely, heme oxygenase-1 (HO-1) expression (see [5] for references). To assess the activation of this signaling cascade in MIO-M1 cells, we tested whether

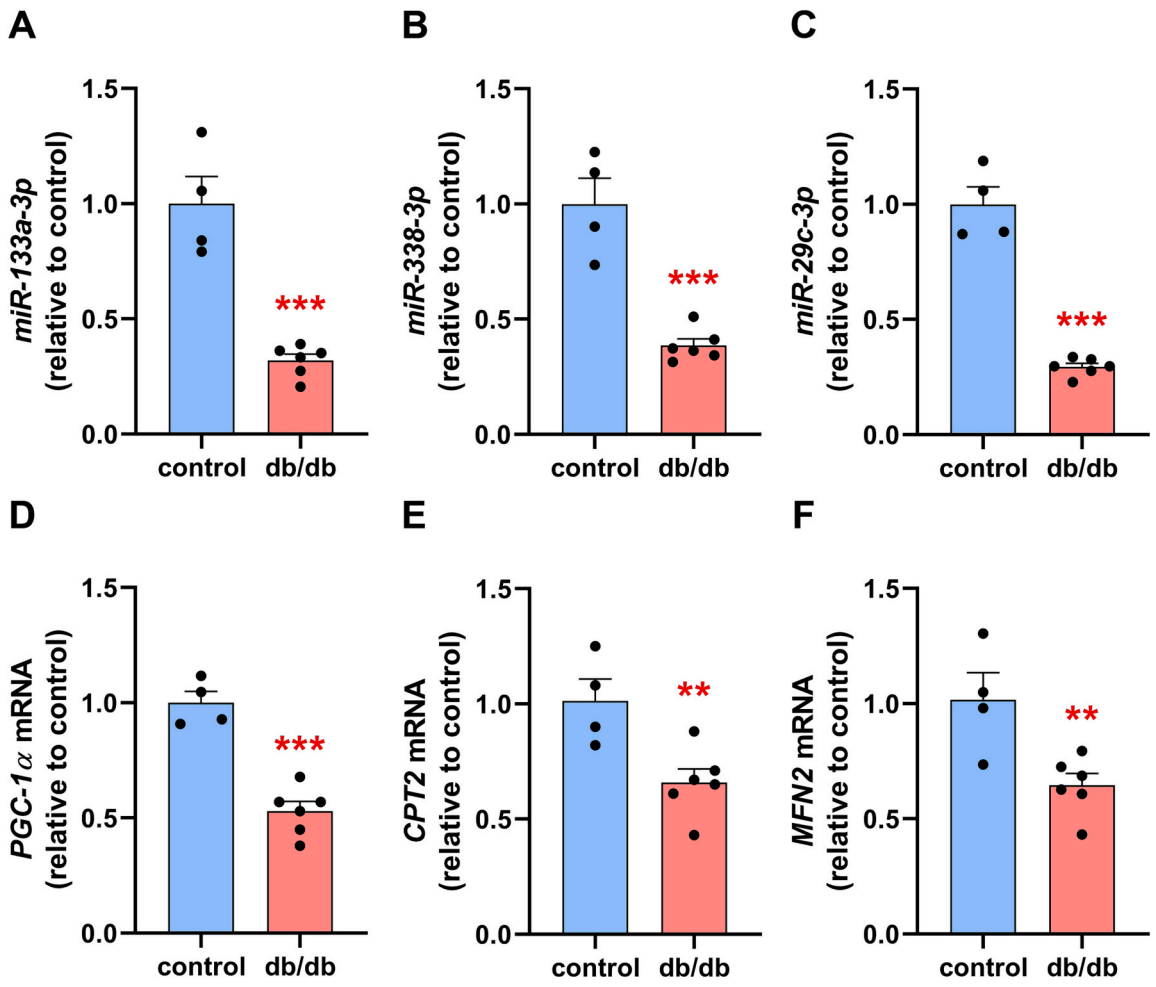

Fig. 5. Expression of miRNAs and of markers of mitochondrial function in retinas of db/db mice at 16 weeks of age compared to co-aged wild type mice (control). The levels of *miR-133a* (A), *miR-338* (B); and *miR-29c* (D) were significantly decreased in db/db retinas. Similarly, the mRNAs of mitochondrial markers *PGC-1α* (D), *CPT2* (E), and *MFN2* (F) were also decreased in db/db retinas. **p < 0.01, ***p < 0.001 vs control.

the HG-driven *DIO3* upregulation could be prevented by inactivation of HIF-1α or of Nrf2 activity in cells cultured in HG for 24 h. As shown in Fig. 6F, the HG-stimulated induction of *DIO3* expression was prevented by co-treatment with either the HIF-1 inhibitor ACF or the Nrf2 inhibitor K67.

3.6. *DIO3 expression is regulated by miR-133a in MIO-M1 cells*

Given that, in db/db mice, the retinal expression of T3-dependent miRNAs (*miR-133a*, *miR-338*, and *miR-29c*) was inversely associated with that of *DIO3*, we assessed whether *DIO3* downregulation could depend on miRNA-mediated transcriptional repression. To test this hypothesis, we firstly conducted an in silico analysis followed by an in vitro validation with reporter gene assay and gain and loss of function experiments. The interaction between *DIO3* and *miR-133a* was predicted in a previous paper [51], where it was demonstrated that *miR-133a* regulates *DIO3* mRNA expression through a 3′UTR dependent mechanism. In the in silico analysis performed here, the search for *mir-29c* binding sites on *DIO3* mRNA gave no results, while *miR-338* resulted as a putative *DIO3* mRNA inhibitor targeting its 3′UTR (Table 1). Therefore, the subsequent in vitro validation experiments were restricted to *miR-133a* and *miR-338*, with the hypothesis that they could mediate T3-induced *DIO3* downregulation.

For the luciferase activity assay in MIO-M1 cells, the entire human 3′UTR of *DIO3* mRNA, containing both the consensus sequence for *miR-133a* and the predicted consensus sequence for *miR-338*, was cloned in a reporter vector downstream of the luciferase gene. We found that *miR-133a* mimic dose-dependently inhibited the expression of the reporter (Fig. 7A), while *miR-338* mimic did not influence the reporter expression (Fig. 7B). The modulatory effect of *miR-133a* was further confirmed by analyzing gene expression variations of *DIO3* in MIO-M1 transfected with *miR-133a* mimic or decoy in the presence or absence of T3 at physiological concentration (3 nM). As shown in Fig. 8C, in the presence of *miR-133a* mimic, the transcript of *DIO3* was significantly reduced, while it was dramatically increased after *miR-133a* inhibition with a decoy sequence. Similar to *miR-133a* mimic, also T3 administration determined a downregulation of *DIO3* mRNA levels, which was prevented in great part by T3 and *mir133a* decoy co-administration. No effects of mimics or decoys for *miR-338* were observed on *DIO3* expression (Fig. 7D).

3.7. *Modulation of T3 influences both MIO-M1 cell response to stress and mitochondrial markers*

The experimental protocol used in these experiments was designed to reproduce the putative scenario occurring in the early phases of DR and to assess the responses of MIO-M1 cells to LT3S correction with T3 replacement. Four groups of treatment were compared (Fig. 8A): 1) a control group, mimicking the physiological condition, was maintained for 14 days in physiological concentration of glucose (5.5 mM) and of T3 (3 nM) (control); 2) a second group, mimicking the initial condition of hyperglycemia with preserved T3 levels, was maintained for 14 days in

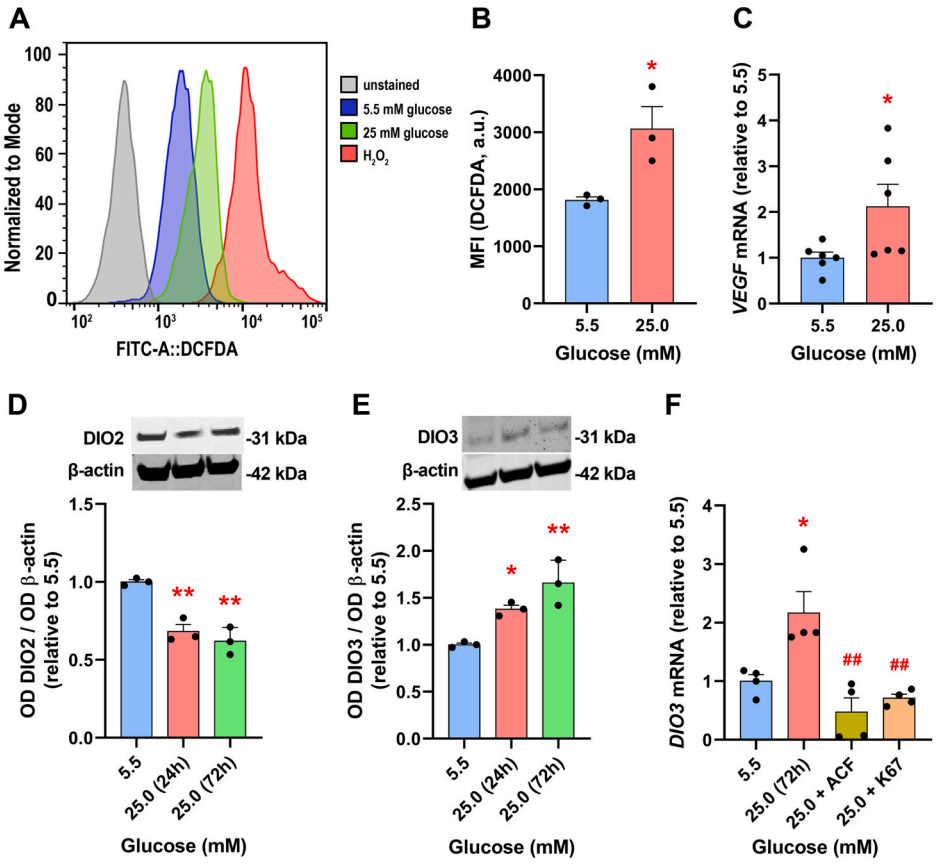

Fig. 6. (A) Representative flow cytometry histograms showing DCFDA-associated fluorescence, indicating the level of ROS production, in MIO-M1 cells incubated for 24 h in physiological glucose concentration (5.5 mM, blue), in HG (25 mM, green), or in 20 mM H_2O_2 (red). Unstained MIO-M1 cells (gray) are also shown. (B) Quantitative evaluation of DFCDA median fluorescence intensity (MFI), expressed in arbitrary units (a.u.), recorded in MIO-M1 cells incubated in normal (5.5 mM) or high (25.0 mM) glucose. (C) *VEGF* mRNA levels evaluated with qPCR in MIO-M1 cells incubated in normal (5.5 mM) or high (25.0 mM) glucose. (D) and (E) show, respectively, immunoreactive bands and protein levels of DIO2 and DIO3 evaluated with Western blotting in MIO-M1 cells incubated in normal (5.5 mM) or high (25.0 mM) glucose for 24 or for 72 h. (F) *DIO3* mRNA expression in MIO-M1 cells incubated for 24 h in normal (5.5 mM) or high (25.0 mM) glucose with or without 5 μM ACF, a HIF inhibitor, or 5 μM K67, a Nrf2 inhibitor. *$p < 0.05$, **$p < 0.01$ vs 5.5 mM glucose; $^{\#\#}p < 0.01$ vs 25.0 mM glucose. (For interpretation of the references to colour in this figure legend, the reader is referred to the web version of this article.)

Table 1
Prediction output for *miR-338*.

Species	miRNA ID	Refseq-id	Start	End
Homo Sapiens	MIMAT0000763	NM_001362.4	973	979
Mus musculus	MIMAT0000582	NM_172119.2	245	260
Rattus Norvegicus	MIMAT0000581	NM_017210	252	258

HG and 3 nM T3 (HG + T3); 3) a third group was maintained for 8 days in HG + T3 followed by 6 days in HG without T3 to mimic the early phase of LT3S (HG-T3); 4) a fourth group, mimicking a T3 replacement procedure, was cultured for 8 days in HG + T3, followed by 3 days in HG–T3, and further three days in HG + T3 (HG-T3 + T3). A stress response, indicated by increased *Nrf2* and *VEGF* mRNA abundance, was observed in the HG + T3 group p (Fig. 8B and C). T3 removal in the HG-T3 group reduced both markers of stress to control levels, while T3 replacement (group HG + T3-T3) provoked a new increase of both parameters. Interestingly, *PGC-1α* and *CPT2*, markers of mitochondrial biogenesis and fatty acid oxidation, showed a similar pattern of expression, with an increase in HG + T3, a decrease to control levels subsequent to T3 removal (HG–T3), and a new rise after T3 replacement (HG–T3 + T3) (Fig. 8D and E).

4. Discussion

Among the stressors participating to neuronal damage in DR, metabolic imbalance due to HG is emerging as a primary factor driving cell suffering. As a consequence, neural cell types with high energy demand, such as RGCs, display important alterations since from early phases of DR. These cells may instate early adaptive responses as an attempt to improve cell resilience, which, instead, may turn into pathological factors with the progression of the disease. In this respect, the overexpression of *VEGF*, the induction of autophagy, and the reorganization of RGC dendritic arborizations have been proposed to represent early cellular responses to the stress provoked by hyperglycemia [1,4,59]. The present study suggests that the regulation of the retinal, local TH system might represent a further adaptive mechanism aimed at preserving cellular energy and reducing metabolic pitfalls after early exposure to HG. Indeed, our results show that in diabetic retinas there is a decrease of TH levels, likely due to a decrease of *DIO2* expression paralleled by an increase of *DIO3* expression, together with a decreased expression of THRs, contributing to the establishment of a LT3S. Our data also show that diabetic retinas are characterized by altered expression of selected miRNAs, suggesting possible mechanisms of deiodinase expression regulation, and of mitochondrial markers, indicating possible consequences of TH alterations on mitochondria. These aspects were further analyzed in vitro using MIO-M1 cell cultures, in which we found HG induced alterations similar to those observed in diabetic mouse retinas

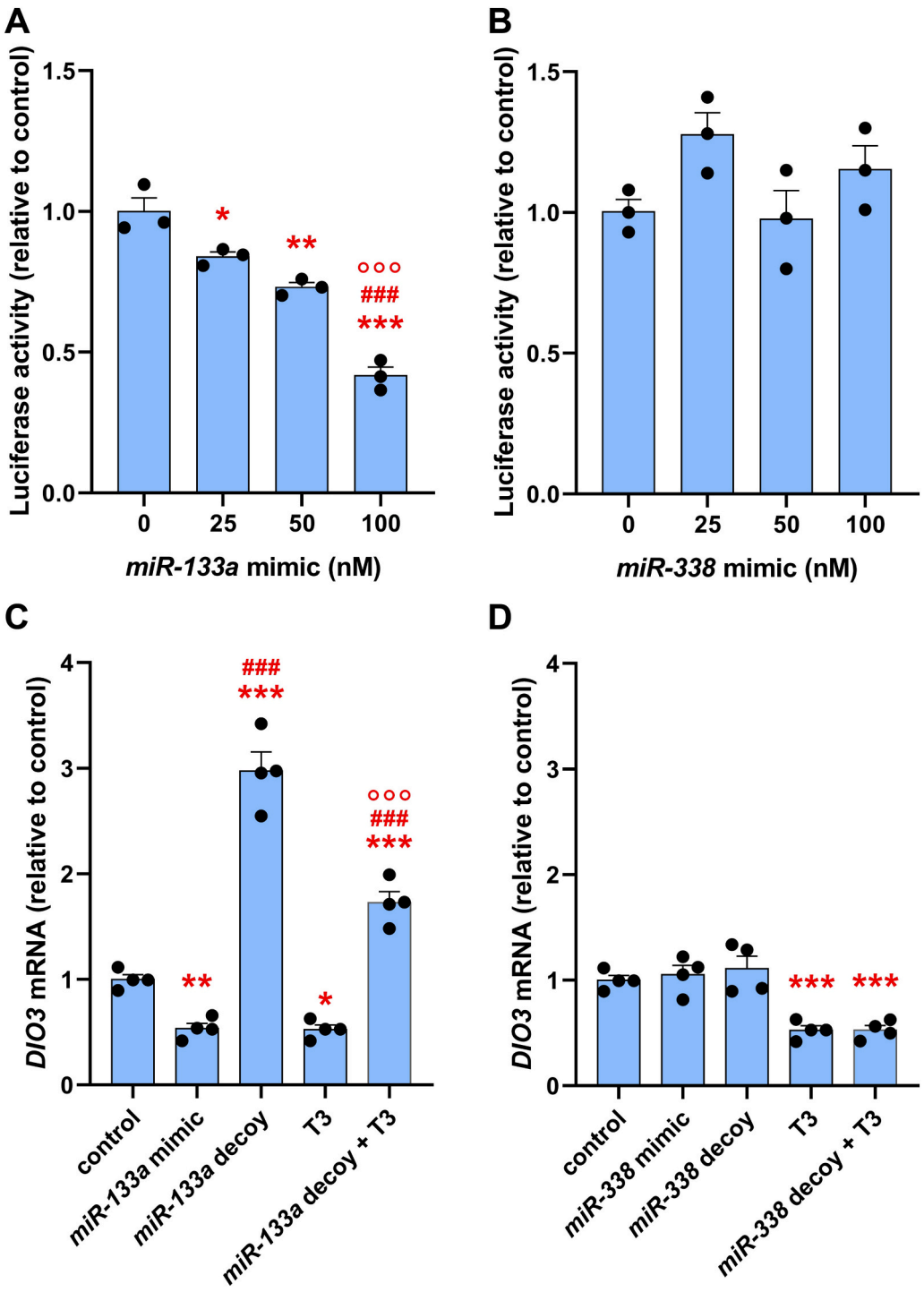

Fig. 7. Modulation of *DIO3* expression by miRNAs. (A) Reporter gene assay showing a dose-dependent inhibition of the luciferase activity by *miR-133a* cotrasfected in MIO-M1 together with a reporter vector in which the entire 3′UTR of *DIO3* has been cloned downstream of the luciferase gene. (B) Luciferase activity assay showing no effect of *miR-338* on the *DIO3* 3′UTR. *$p < 0.05$, **$p < 0.01$, ***$p < 0.001$ vs control; $^{\#}p < 0.05$, $^{\#\#\#}p < 0.001$ vs 25 nM; $^{\circ\circ\circ}p < 0.001$ vs 50 nM. N = 3. (C) *DIO3* mRNA expression (relative to control) in MIO-M1 cells incubated for 48 h with 100 nM *miR-133a* mimic or 100 nM *miR-133a* decoy, in the presence or absence of 3 nM T3. (D) *DIO3* mRNA expression (relative to control) in MIO-M1 cells incubated for 48 h in the presence of 100 nM *miR-338* mimic or 100 nM *miR-338* decoy, in the presence or absence of 3 nM T3. The data relative to control mimic and those of control 2′*O*-methylated decoy were almost identical, therefore for the analysis we choose to consider only one control group (made by the mean of the two control groups). *$p < 0.05$, **$p < 0.01$, ***$p < 0.001$ vs control; $^{\#\#\#}p < 0.001$ vs *miR-133a* mimic; $^{\circ\circ\circ}p < 0.001$ vs *miR-133a* decoy.

and in which we detected a feedback regulatory mechanism involving *miR133a* and leading to *DIO3* upregulation through a Nrf2 - HIF-1 dependent pathway. Finally, in an in vitro experimental setup with MIO-M1 cells mimicking a condition of early DR, we found that T3 removal (mimicking LT3S) reduced, while T3 replacement increased, the retinal stress induced by HG.

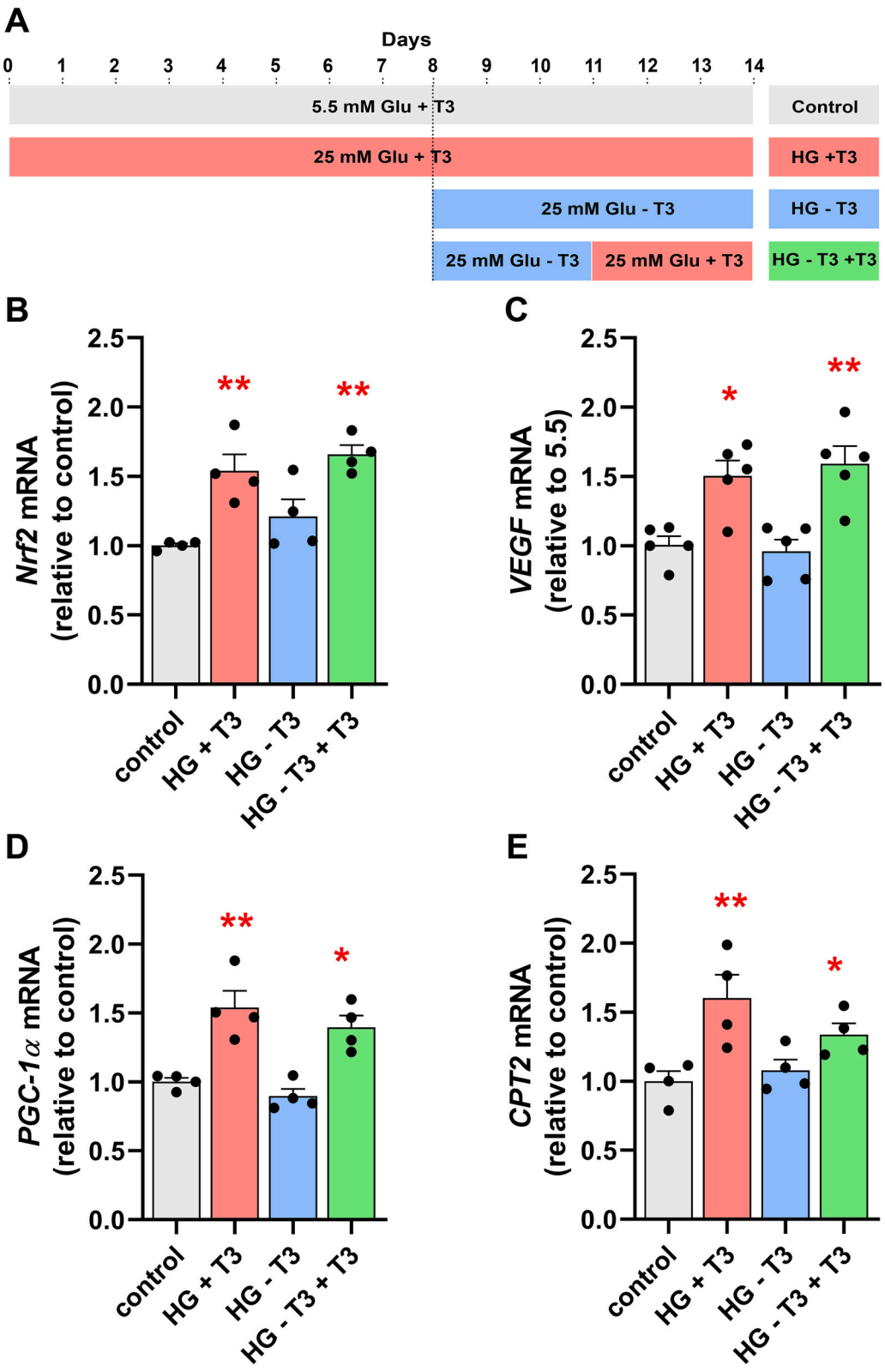

Fig. 8. Effects of the presence/withdrawal/replacement of T3 on cellular stress and on mitochondrial function in MIO-M1 cells cultured in HG. (A) Experimental setup: MIO-M1 cells were grown in normal (5.5 mM) glucose in the presence of 3 nM T3 (control). At experiment onset, one group of cells was exposed to high (25 mM) glucose (HG) and was cultured in this condition for 8 days. The first experimental group (HG + T3) was cultured for the subsequent 6 days (total = 14 days) in the same condition (25 mM glucose, 3 nM T3). The second experimental group (HG-T3) was cultured for the last 6 days in a medium devoid of T3 (LT3S mimic). In the third experimental group (HG-T3 + T3), T3 was removed from the medium after the first 8 days and was replaced after 3 further days of incubation until day 14 (LT3S mimic plus T3 replacement). Oxidative stress (evaluated with *Nrf2* mRNA expression, B) and *VEGF* mRNA expression (C) were increased in the HG + T3 group, they were reduced to control levels in the HG-T3 group and were increased again in the HG-T3 + T3 group. Similar patterns were observed in the expression of the mitochondrial markers *PGC-1α* (D) and *CPT2* (E) mRNAs. *$p < 0.05$, **$p < 0.01$ vs control.

4.1. Pathological hallmarks of DR correlate with altered TH signaling at local level

Clinical studies indicate a negative correlation between circulating TH levels and risk of developing DR [24–26,60], although there are also reports indicating that thyroid dysfunction does not have any link with diabetic complications, including DR [61]. In order to clarify possible relationships between the TH system and DR progression, we correlated plasma and retinal levels of TH with major hallmarks of DR in the db/db mouse model of type 2 diabetes mellitus.

The db/db mouse has been used as a model of DR in a number of studies, which provided a variety of data for the characterization of the retinas of these mice. In particular, our scERG analyses are consistent with those of previous findings in db/db mice aged 9–28 weeks demonstrating decreased amplitudes and increased implicit times of a- and b-waves mainly elicited by the rod-mediated pathway [42,62–66]. In addition, our data provide further evidence of altered cone-mediated pathway as demonstrated by decreased phERG b-wave and PhNR amplitudes in db/db retinas. Dysfunctional rod- and cone-mediated pathways resulted in altered RGC activity, as demonstrated by decreased PERG responses, previously observed also in db/db mice aged 28 weeks [59]. Altered retinal activity correlated with typical molecular changes occurring over DR progression such as reactive gliosis, the increase in oxidative stress, inflammation, and *VEGF* expression, and the decrease of tight junction protein *ZO1*, in line with previous observations [41,42,62,64,67–70]. In addition, retinal thickening [41] or thinning [42,71], apoptosis in the RGC layer [42,62,67], glutamate/aspartate transporter downregulation and glutamate accumulation [42,62], and microvascular changes [62,64,70,72], including some vessel proliferation in the most aged mice [70], were also reported in db/db retinas. In summary, our observations, together with previously published data, allow to establish that at 16 weeks of age, db/db mice are affected by DR and that their retinas are characterized by marked functional deficits at the level of both the outer and the inner retina, increased oxidative stress and inflammation, *VEGF* overexpression, and BRB breakdown. In addition, the present work provides novel evidence of the presence of a LT3S in these retinas.

The occurrence of DR hallmarks in db/db mice appeared to be independent from changes in T3 or T4 plasma levels, at least at 16 weeks of age, since no differences were recorded between the circulating TH levels of db/db mice and those of controls. In contrast, we observed a LT3S within the retina, with marked decreases of both T3 and T4 concentrations, suggesting that important TH-based mechanisms are likely to take place within the retina and influence the development of DR independent of circulating TH. The possibility of a local control of TH signaling in the retina is in line with a number of observations. For instance, a mechanism has been described recently in which the control of TH signaling among different retinal cell types plays a pivotal role in light/dark adaptation [73] and, in general, there is evidence indicating that deiodinases can regulate intracellular TH levels, in both animals and humans, independent of systemic TH [74]. In particular, TH can be deiodinated by three different deiodinases (DIO1, DIO2 and DIO3). Both DIO1 and DIO2 convert the prohormone T4 into the active hormone T3, thereby increasing TH signaling, while DIO3 converts T4 and T3 into rT3 and 3,5-diiodothyronine (T2), respectively, both of which have only low affinity for THR [75]. Thus, deiodinase enzymes in target cells regulate T3 availability and provide a tissue-specific level of regulation of TH signaling. As demonstrated by the present results, local LT3S in db/db retinas correlates with increased DIO3 expression and decreased DIO2 expression, suggesting a reprogramming of the retinal TH system towards a decrease of T4 conversion into T3 and an increase of the inactive forms rT3 and T2, resulting in overall reduction of TH signaling.

Delving into DIO2 in db/db retinas, we observed that the reduction of its mRNA expression was much more pronounced than that of DIO2 protein. This discrepancy could be attributed to the complex post-transcriptional regulation of *DIO2* gene expression. Indeed, *DIO2* mRNA, on the one hand undergoes alternative splicing, and on the other it contains both 3′ and 5′ untranslated regions harboring regulative elements (some open reading frames and adenine- and uracil-rich elements, respectively) that impact on the mRNA half-life and translation efficacy [76]. These mechanisms could be dysregulated in the retina during DR, altering the *DIO2* mRNA to protein ratio.

A reduced T3 signaling in the diabetic retina is likely to be induced not only by an increased DIO3 expression, but also by THR downregulation. Indeed, our data report significant decreases of both *THRα1* and *THRβ2* expression. Changes in THR expression have been reported also in the diabetic kidney and in stressed cardiomyocytes, however in these cases the observed changes included an increased expression of THRα that was interpreted as a fetal reprogramming aimed at providing metabolic benefits to the stressed tissues [28]. In line with previous results in a model of brain ischemia [77], our observations indicate that in the retinas of db/db mice the response of the THR system to stress seems to be different from that in other organs.

4.2. Oxidative stress and HIF-1α regulate DIO3 levels under HG

The evidence provided in the present studies indicates that DIO3 is the main responsible for the induction of a LT3S in the diabetic retina, similar to previous observations in the ischemic heart [51,58]. In the setting of cardiac ischemia, a mechanism of metabolic regulation during hypoxic-ischemic injury has been clarified, in which induction of *DIO3* with consequent reduction of local TH signaling is promoted by HIF-1 [58]. Since HIF-1 is known to play a central role in DR [5,78], we hypothesized that the decrease of T3 levels observed in db/db retinas is due to HIF-1-mediated increase of *DIO3* expression. This hypothesis was tested using an in vitro model of MIO-M1 cells exposed to HG, which displayed alterations in oxidative balance and *VEGF* expression together with a significant upregulation of *DIO3,* well resembling the in vivo condition. Noteworthy, blockade of HIF-1 prevented the HG-induced increase of *DIO3* mRNA expression, thus confirming a role of HIF-1 on *DIO3* upregulation. In addition, our previous observations indicated that HIF-1α stabilization, necessary for the formation of HIF-1, may be caused, among other factors, by Nrf2 activation [5] and the existence of an intracellular Nrf2 - HIF-1 pathway regulating *DIO3* expression is consistent with the observation reported here that Nrf2 blockade abolishes *DIO3* mRNA overexpression in MIO-M1 cells cultured in HG. In summary, the data of the present study, together with those of previous investigations, suggest a mechanism like the one depicted in Fig. 9, where HG-induced oxidative stress would activate Nrf2, which, likely through an increase of HO-1 expression (see [5] for references), would promote HIF-1α stabilization, resulting in increased DIO3 expression and LT3S.

4.3. A regulatory feedback mechanism involving miR-133a regulates T3-dependent DIO3 expression

It is increasingly recognized that T3-dependent miRNAs are involved in post transcriptional regulation of a variety of genes relevant to organ physiology and pathophysiology [79]. For instance, in a model of acute myocardial infarction in rats, *miR-133a*, *miR-338*, and *miR-29c* downregulation has been found to correlate with LT3S, with T3 replacement resulting effective in restoring miRNA levels [31]. Interestingly, these miRNAs were also downregulated in db/db retinas, suggesting their possible involvement in altered TH signaling. Among these miRNAs, *miR-133a* and *miR-338* were predicted to regulate DIO3 protein levels through translational inhibition, thus raising the possibility that DIO3 might also be regulated by a T3-dependent feedback loop through specific miRNAs. Our results obtained with the luciferase reporter assay show that *miR-133a*, but not *miR-338*, can post-trascriptionally repress *DIO3* in MIO-M1 cells. This observation is confirmed by the opposite changes of *DIO3* mRNA abundance after administration of a *miR-133a* mimic or decoy. Our findings also show a downregulation of *DIO3*

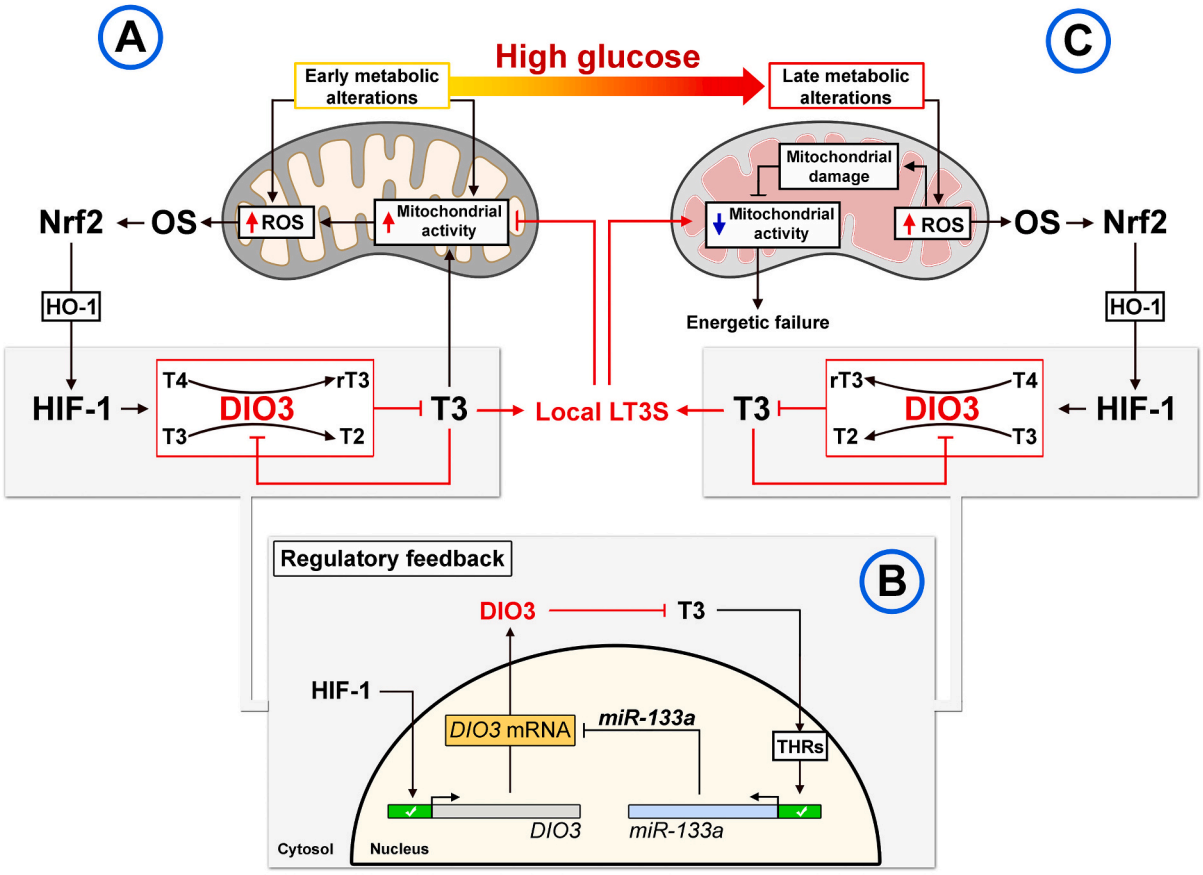

Fig. 9. Graphical representation of the proposed mechanisms for TH system modulation in retinal cells under diabetic conditions and its relevance for metabolic stress. (A) In early phases of DR, the exposure to HG is likely to trigger early metabolic alterations driving mitochondrial hyperactivity, thus increasing ROS production and oxidative stress (OS), which would trigger Nrf2 activation and the expression of antioxidant enzymes. Among them, HO-1 may mediate the cross-activation of HIF-1, which would act as a transcriptional activator of *DIO3*. Consequently, *DIO3* upregulation would alter TH balance by promoting both the conversion of T4 into rT3 and that of T3 into T2. As a result, the levels of the active hormone T3 would decrease and instate a local LT3S. (B) The drop in T3 levels would promote further DIO3 upregulation, since the decreased activation of THRs would lead to down-regulation of *miR133a* and consequent decrease of its inhibitory effect on DIO3 expression. The reduced T3-dependent negative feedback on DIO3 expression would sustain a self-feeding loop enhancing local LT3S in retinal cells over DR progression. In early stages, LT3S would represent a compensatory response to repress excessive mitochondrial activity. However (C), the long-lasting repression of mitochondrial activity by LT3S might exacerbate the belated mitochondrial dysfunction due to ROS-driven damage, thus promoting energetic failure.

expression following T3 administration and a partial reversal of this effect by blockade of *miR-133a* function. Together, these observations are consistent with a T3-mediated inhibitory action of *DIO3* expression mediated by *miR-133a* (Fig. 9). The residual induction of *DIO3* following T3 and *miR-133a* decoy co-treatment, suggests that *DIO3* levels may be regulated by multiple T3-dependent pathways.

4.4. LT3S may affect the retinal response to stress through an action on mitochondrial function

In db/db mice, the retinal LT3S is concomitant with important alterations of genes relevant to mitochondrial function, as evidenced by significant decreases of *PGC-1α*, *CPT2*, and *MFN2* expressions. PGC-1α plays a central role in mitochondrial biogenesis through the activation of different transcription factors in response to stimuli such as cold or exercise [47,55]. This factor is known to be regulated by T3 [79,80] and it has been reported to mediate the growth-promoting activity of T3 in developing Purkinje cells [81]. CPT2 cooperates with CPT1 in the fatty acid oxidation pathway in the mitochondria [56] and the expression of both enzymes is under the control of T3 [82,83]. MFN2 is a key player in a variety of mitochondrial functions [84] that are known to be influenced by TH [85]. Collectively, our observations indicate that the mitochondrial impairment highlighted by changes in *PGC-1α*, *CPT1* and *MFN2* expressions is likely to be caused, at least in part, by the occurrence of a LT3S.

The experiments in which MIO-M1 cells were cultured with or without T3 represent a condition that is likely to characterize the early phases of DR. Our observations show that HG induces a stress response in MIO-M1 cells (increased ROS and *VEGF* expression) only in the presence of T3. Therefore, a LT3S in early phases seems to have beneficial effects, while T3 replacement at these times is likely to worsen the cellular stress response. The data also show that T3 affects mitochondrial markers of biogenesis and fatty acid oxidation, suggesting that the effects of T3 on cellular stress are likely to be mediated by modulation of mitochondrial function. .In the long term (as shown by our observations in db/db retinas), the parameters of mitochondrial biogenesis and function are low, but the stress parameters (oxidative stress, inflammation, *VEGF* expression, and BRB damage) are increased, suggesting that prolonged mitochondrial inhibition caused by LT3S loses its beneficial effects and in the chronic phase it becomes detrimental. Data in the literature indicate that retinal mitochondria in diabetes are characterized by early and transient activation followed by later decline [86]. The findings of the present work provide evidence that local TH regulation and LT3S are likely to play central roles in these phenomena.

5. Conclusions

The present studies demonstrate for the first time a local LT3S in the diabetic retina. Among TH, we have focused on the biological significance of local T3 lowering in the retina, as T3 is widely known as the biologically active form of TH. However, the concurrent decrement in local T4 levels, as observed in db/db retinas, may also play a role in the TH-dependent response to HG-induced stress, which will deserve attention in future studies.

As summarized in Fig. 9, our data suggest a feedback mechanism in which DIO3 expression is regulated by T3 levels through mediation of *miR-133a* (and likely of other factors). This mechanism would be altered by hyperglycemia, which causes oxidative stress, HIF-1α stabilization, and, consequently, DIO3 upregulation. As shown by our data, the resulting LT3S causes a decrease of some mitochondrial markers, which we may interpret as a sign of impaired mitochondrial function, a condition that, in early phases of DR, would help the tissue against the stress caused by HG. Interestingly, a T3 replacement strategy in this phase may remove the beneficial effect of LT3S and restore the damaging effects of HG. However, in the chronic phase LT3S is no longer associated with retinal protection. It is reasonable to hypothesize that prolonged mitochondrial dysfunction, caused by persistent LT3S, not only fails to limit the HG-induced damage, but also renders the cells more vulnerable due to decreased metabolic homeostasis. Although in other scenarios a T3 replacement strategy may have a therapeutic value [29,30], this does not seem to be the case in DR, at least in the early phases of the disease. Whether such strategy may have beneficial effects at later stages of DR remains to be elucidated with further investigations.

Funding

This research did not receive any specific grant from funding agencies in the public, commercial, or not-for-profit sectors. It was supported by general funding from Italian Ministry of University and Research.

CRediT authorship contribution statement

Francesca Forini: Conceptualization, Methodology, Validation, Formal analysis, Investigation, Resources, Writing – original draft, Writing – review & editing, Supervision, Project administration. **Giuseppina Nicolini:** Conceptualization, Methodology, Formal analysis, Investigation, Writing – review & editing, Project administration. **Rosario Amato:** Conceptualization, Methodology, Validation, Formal analysis, Investigation, Writing – review & editing, Project administration. **Silvana Balzan:** Conceptualization, Methodology, Formal analysis, Resources, Writing – review & editing, Funding acquisition. **Alessandro Saba:** Formal analysis, Investigation, Resources, Writing – review & editing. **Andrea Bertolini:** Investigation. **Elena Andreucci:** Investigation. **Silvia Marracci:** Formal analysis, Investigation. **Alberto Melecchi:** Formal analysis, Investigation. **Domiziana Terlizzi:** Resources. **Riccardo Zucchi:** Resources, Funding acquisition. **Giorgio Iervasi:** Resources, Writing – review & editing, Funding acquisition. **Matteo Lulli:** Conceptualization, Methodology, Validation, Formal analysis, Investigation, Resources, Writing – original draft, Writing – review & editing, Supervision, Project administration, Funding acquisition. **Giovanni Casini:** Conceptualization, Methodology, Validation, Formal analysis, Resources, Writing – original draft, Writing – review & editing, Supervision, Project administration, Funding acquisition.

Declaration of competing interest

The authors declare no conflicts of interest.

Data availability

Data will be made available on request.

Acknowledgements

- The Centre for Instrumentation Sharing of University of Pisa (CISUP) is kindly acknowledged for providing the Sciex QTrap 6500+ mass spectrometer used for the mass spectrometric assays. The authors are grateful to Dr. Giorgio Soldani, Institute of Clinical Physiology, for providing the retinas of db/db mice. The authors also thank Dr. Maria Grazia Rossino for her help in the initial phases of this study.

Appendix A. Supplementary data

Supplementary data to this article can be found online at https://doi.org/10.1016/j.bbadis.2023.166892.

References

[1] R. Amato, E. Catalani, M. Dal Monte, M. Cammalleri, D. Cervia, G. Casini, Morpho-functional analysis of the early changes induced in retinal ganglion cells by the onset of diabetic retinopathy: the effects of a neuroprotective strategy, Pharmacol. Res. 185 (2022) 106516, https://doi.org/10.1016/j.phrs.2022.106516.
[2] C. Hernández, M. Dal Monte, R. Simó, G. Casini, Neuroprotection as a therapeutic target for diabetic retinopathy, J. Diabetes Res. 2016 (2016) 9508541, https://doi.org/10.1155/2016/9508541.
[3] M.G. Rossino, M. Dal Monte, G. Casini, Relationships between neurodegeneration and vascular damage in diabetic retinopathy, Front. Neurosci. 13 (2019) 1172, https://doi.org/10.3389/fnins.2019.01172.
[4] R. Amato, M. Biagioni, M. Cammalleri, M. Dal Monte, G. Casini, VEGF as a survival factor in ex vivo models of early diabetic retinopathy, Invest. Ophthalmol. Vis. Sci. 57 (2016) 3066–3076, https://doi.org/10.1167/iovs.16-19285.
[5] M.G. Rossino, M. Lulli, R. Amato, M. Cammalleri, M.D. Monte, G. Casini, Oxidative stress induces a VEGF autocrine loop in the retina: relevance for diabetic retinopathy, Cells 9 (2020) 1452, https://doi.org/10.3390/cells9061452.
[6] Q. Gong, H. Wang, P. Yu, T. Qian, X. Xu, Protective or harmful: the dual roles of autophagy in diabetic retinopathy, Front. Med. 8 (2021) 644121, https://doi.org/10.3389/fmed.2021.644121.
[7] F. Forini, G. Nicolini, C. Kusmic, G. Iervasi, Protective effects of euthyroidism restoration on mitochondria function and quality control in cardiac pathophysiology, Int. J. Mol. Sci. 20 (2019) 3377, https://doi.org/10.3390/ijms20143377.
[8] F. Cioffi, A. Giacco, F. Goglia, E. Silvestri, Bioenergetic aspects of mitochondrial actions of thyroid hormones, Cells 11 (2022) 997, https://doi.org/10.3390/cells11060997.
[9] C. Wrutniak-Cabello, F. Casas, G. Cabello, Thyroid hormone action in mitochondria, J. Mol. Endocrinol. 26 (2001) 67–77, https://doi.org/10.1677/jme.0.0260067.
[10] F. Flamant, J.D. Baxter, D. Forrest, S. Refetoff, H. Samuels, T.S. Scanlan, B. Vennström, J. Samarut, International Union of Pharmacology. LIX. The pharmacology and classification of the nuclear receptor superfamily: thyroid hormone receptors, Pharmacol. Rev. 58 (2006) 705–711, https://doi.org/10.1124/pr.58.4.3.
[11] L. Ng, M. Ma, T. Curran, D. Forrest, Developmental expression of thyroid hormone receptor beta2 protein in cone photoreceptors in the mouse, Neuroreport 20 (2009) 627–631, https://doi.org/10.1097/WNR.0b013e32832a2c63.
[12] L. Ng, H. Liu, Y. Liu, D. Forrest, Biphasic expression of thyroid hormone receptor TRβ1 in mammalian retina and anterior ocular tissues, Front. Endocrinol. (Lausanne) 14 (Mar 23, 2023), 1174600, https://doi.org/10.3389/fendo.2023.1174600.
[13] Y. Henning, K. Szafranski, Age-dependent changes of monocarboxylate transporter 8 availability in the postnatal murine retina, Front. Cell. Neurosci. 10 (2016) 205, https://doi.org/10.3389/fncel.2016.00205.
[14] P. Arbogast, F. Flamant, P. Godement, M. Glösmann, L. Peichl, Thyroid hormone signaling in the mouse retina, PLoS One 11 (2016), 0168003, https://doi.org/10.1371/journal.pone.0168003.
[15] L. Ng, A. Lyubarsky, S.S. Nikonov, M. Ma, M. Srinivas, B. Kefas, D.L. St Germain, A. Hernandez, E.N. Pugh Jr., D. Forrest, Type 3 deiodinase, a thyroid-hormone-inactivating enzyme, controls survival and maturation of cone photoreceptors, J. Neurosci. 30 (2010) 3347–3357, https://doi.org/10.1523/JNEUROSCI.5267-09.2010.
[16] O. Sawant, A.M. Horton, M. Shukla, M.E. Rayborn, N.S. Peachey, J.G. Hollyfield, S. Rao, Light-regulated thyroid hormone signaling is required for rod photoreceptor development in the mouse retina, Invest. Ophthalmol. Vis. Sci. 56 (2015) 8248–8257, https://doi.org/10.1167/iovs.15-17743.
[17] H. Ma, F. Yang, M.R. Butler, J. Belcher, T.M. Redmond, A.T. Placzek, T.S. Scanlan, X.Q. Ding, Inhibition of thyroid hormone receptor locally in the retina is a

therapeutic strategy for retinal degeneration, FASEB J. 31 (2017) 3425–3438, https://doi.org/10.1096/fj.201601166RR.
[18] F. Yang, H. Ma, J. Belcher, M.R. Butler, T.M. Redmond, S.L. Boye, W.W. Hauswirth, X.Q. Ding, Targeting iodothyronine deiodinases locally in the retina is a therapeutic strategy for retinal degeneration, FASEB J. 30 (2016) 4313–4325, https://doi.org/10.1096/fj.201600715R.
[19] F. Yang, H. Ma, M.R. Butler, X.Q. Ding, Deficiency of type 2 iodothyronine deiodinase reduces necroptosis activity and oxidative stress responses in retinas of Leber congenital amaurosis model mice, FASEB J. 32 (2018), fj201800484RR, https://doi.org/10.1096/fj.201800484RR.
[20] R. Gao, R.Z. Chen, Y. Xia, J.H. Liang, L. Wang, H.Y. Zhu, J. Zhu Wu, L. Fan, J.Y. Li, T. Yang, W. Xu, Low T3 syndrome as a predictor of poor prognosis in chronic lymphocytic leukemia, Int. J. Cancer 143 (2018) 466–477, https://doi.org/10.1002/ijc.31327.
[21] J.C. Lo, G.M. Chertow, A.S. Go, C.Y. Hsu, Increased prevalence of subclinical and clinical hypothyroidism in persons with chronic kidney disease, Kidney Int. 67 (2005) 1047–1052, https://doi.org/10.1111/j.1523-1755.2005.00169.x.
[22] G.Q. Huang, Y.Y. Zeng, Q.Q. Cheng, H.R. Cheng, Y.T. Ruan, C.X. Yuan, Y.B. Chen, W.L. He, H.J. Chen, J.C. He, Low triiodothyronine syndrome is associated with hemorrhagic transformation in patients with acute ischaemic stroke, Aging 11 (2019) 6385–6397, https://doi.org/10.18632/aging.102195.
[23] G. Iervasi, A. Pingitore, P. Landi, M. Raciti, A. Ripoli, M. Scarlattini, A. L'Abbate, L. Donato, Low-T3 syndrome: a strong prognostic predictor of death in patients with heart disease, Circulation 107 (2003) 708–713, https://doi.org/10.1161/01.cir.0000048124.64204.3f.
[24] Z. Heidari, R. Asadzadeh, Subclinical hypothyroidism is a risk factor for diabetic retinopathy in patients with type 2 diabetes mellitus, Med. J. Islam Repub. Iran 35 (186) (2021), https://doi.org/10.47176/mjiri.35.186.
[25] Y. Hu, Z. Hu, W. Tang, W. Liu, X. Wu, C. Pan, Association of thyroid hormone levels with microvascular complications in euthyroid type 2 diabetes mellitus patients, Diabetes Metab. Syndr. Obes. 15 (2022) 2467–2477, https://doi.org/10.2147/DMSO.S354872.
[26] X. Kong, J. Wang, G. Gao, M. Tan, B. Ding, H. Li, J. Ma, Association between free thyroxine levels and diabetic retinopathy in euthyroid patients with type 2 diabetes mellitus, Endocr. Res. 45 (2020) 111–118, https://doi.org/10.1080/07435800.2019.1690504.
[27] P. Mantzouratou, A.M. Lavecchia, R. Novelli, C. Xinaris, Thyroid hormone signalling alteration in diabetic nephropathy and cardiomyopathy: a "switch" to the foetal gene programme, Curr. Diab. Rep. 20 (2020) 020–01344, https://doi.org/10.1007/s11892-020-01344-6.
[28] G. Nicolini, F. Forini, C. Kusmic, L. Pitto, L. Mariani, G. Iervasi, Early and short-term triiodothyronine supplementation prevents adverse postischemic cardiac remodeling: role of transforming growth factor-β1 and antifibrotic miRNA signaling, Mol. Med. 21 (2016) 900–911, https://doi.org/10.2119/molmed.2015.00140.
[29] F. Forini, C. Kusmic, G. Nicolini, L. Mariani, R. Zucchi, M. Matteucci, G. Iervasi, L. Pitto, Triiodothyronine prevents cardiac ischemia/reperfusion mitochondrial impairment and cell loss by regulating miR30a/p53 axis, Endocrinology 155 (2014) 4581–4590, https://doi.org/10.1210/en.2014-1106.
[30] F. Forini, G. Nicolini, C. Kusmic, R. D'Aurizio, M. Rizzo, M. Baumgart, M. Groth, S. Doccini, G. Iervasi, L. Pitto, Integrative analysis of differentially expressed genes and miRNAs predicts complex T3-mediated protective circuits in a rat model of cardiac ischemia reperfusion, Sci. Rep. 8 (2018) 018–32237, https://doi.org/10.1038/s41598-018-32237-0.
[31] A. Pingitore, F. Mastorci, P. Piaggi, G.D. Aquaro, S. Molinaro, M. Ravani, A. De Caterina, G. Trianni, R. Ndreu, S. Berti, C. Vassalle, G. Iervasi, Usefulness of triiodothyronine replacement therapy in patients with ST elevation myocardial infarction and borderline/reduced triiodothyronine levels (from the THIRST study), Am. J. Cardiol. 123 (6) (Mar 15, 2019) 905–912, https://doi.org/10.1016/j.amjcard.2018.
[32] A.G. Little, Local regulation of thyroid hormone signaling, Vitam. Horm. 106 (2018) 1–17, https://doi.org/10.1016/bs.vh.2017.06.004.
[33] A.G. Cicatiello, D. Di Girolamo, M. Dentice, Metabolic effects of the intracellular regulation of thyroid hormone: old players, new concepts, Front. Endocrinol. (Lausanne) 9 (Sep 11, 2018) 474, https://doi.org/10.3389/fendo.2018.00474.
[34] C. Vale, J.S. Neves, M. von Hafe, M. Borges-Canha, A. Leite-Moreira, The role of thyroid hormones in heart failure, Cardiovasc. Drugs Ther. 33 (2) (2019 Apr) 179–188, https://doi.org/10.1007/s10557-019-06870-4.
[35] E. Sawano, T. Negishi, T. Aoki, M. Murakami, T. Tashiro, Alterations in local thyroid hormone signaling in the hippocampus of the SAMP8 mouse at younger ages: association with delayed myelination and behavioral abnormalities, J. Neurosci. Res. 91 (3) (2013 Mar) 382–392, https://doi.org/10.1002/jnr.23161.
[36] B. Gereben, A.M. Zavacki, S. Ribich, B.W. Kim, S.A. Huang, W.S. Simonides, A. Zeöld, A.C. Bianco, Cellular and molecular basis of deiodinase-regulated thyroid hormone signaling, Endocr. Rev. 29 (7) (Dec 2008) 898–938, https://doi.org/10.1210/er.2008-0019.
[37] R. Mastropasqua, L. Toto, F. Cipollone, D. Santovito, P. Carpineto, L. Mastropasqua, Role of microRNAs in the modulation of diabetic retinopathy, Prog. Retin. Eye Res. 43 (2014) 92–107, https://doi.org/10.1016/j.preteyeres.2014.07.003.
[38] R. Shafabakhsh, E. Aghadavod, M. Mobini, R. Heidari-Soureshjani, Z. Asemi, Association between microRNAs expression and signaling pathways of inflammatory markers in diabetic retinopathy, J. Cell. Physiol. 234 (2019) 7781–7787, https://doi.org/10.1002/jcp.27685.
[39] Z. Smit-McBride, L.S. Morse, MicroRNA and diabetic retinopathy-biomarkers and novel therapeutics, Ann. Transl. Med. 9 (2021) 20–5189, https://doi.org/10.21037/atm-20-5189.
[40] R.A. Kowluru, Mitochondrial stability in diabetic retinopathy: lessons learned from epigenetics, Diabetes 68 (2019) 241–247, https://doi.org/10.2337/dbi18-0016.
[41] T. Azrad-Leibovich, A. Zahavi, M.F. Gohas, M. Brookman, O. Barinfeld, O. Muhsinoglu, S. Michowiz, D. Fixler, N. Goldenberg-Cohen, Characterization of diabetic retinopathy in two mouse models and response to a single injection of anti-vascular endothelial growth factor, Int. J. Mol. Sci. 24 (2022) 324, https://doi.org/10.3390/ijms24010324.
[42] P. Bogdanov, L. Corraliza, J.A. Villena, A.R. Carvalho, J. Garcia-Arumí, D. Ramos, J. Ruberte, R. Simó, C. Hernández, The db/db mouse: a useful model for the study of diabetic retinal neurodegeneration, PLoS One 9 (2014), e97302, https://doi.org/10.1371/journal.pone.0097302.
[43] K. Szabadfi, E. Pinter, D. Reglodi, R. Gabriel, Neuropeptides, trophic factors, and other substances providing morphofunctional and metabolic protection in experimental models of diabetic retinopathy, Int. Rev. Cell Mol. Biol. 311 (2014) 1–121, https://doi.org/10.1016/B978-0-12-800179-0.00001-5.
[44] P. Losi, T. Al Kayal, M. Buscemi, I. Foffa, A. Cavallo, G. Soldani, Bilayered fibrin-based electrospun-sprayed scaffold loaded with platelet lysate enhances wound healing in a diabetic mouse model, Nanomaterials 10 (2020) 2128, https://doi.org/10.3390/nano10112128.
[45] E. Agardh, A. Bruun, C.D. Agardh, Retinal glial cell immunoreactivity and neuronal cell changes in rats with STZ-induced diabetes, Curr. Eye Res. 23 (4) (Oct 2001) 276–284, https://doi.org/10.1076/ceyr.23.4.276.5459. 11852429.
[46] A. Saba, R. Donzelli, D. Colligiani, A. Raffaelli, M. Nannipieri, C. Kusmic, C.G. Dos Remedios, W.S. Simonides, G. Iervasi, R. Zucchi, Quantification of thyroxine and 3,5,3′-triiodo-thyronine in human and animal hearts by a novel liquid chromatography-tandem mass spectrometry method, Horm. Metab. Res. 46 (2014) 628–634, https://doi.org/10.1055/s-0034-1368717.
[47] R. Donzelli, D. Colligiani, C. Kusmic, M. Sabatini, L. Lorenzini, A. Accorroni, M. Nannipieri, A. Saba, G. Iervasi, R. Zucchi, Effect of hypothyroidism and hyperthyroidism on tissue thyroid hormone concentrations in rat, Eur. Thyroid J. 5 (2016) 27–34, https://doi.org/10.1159/000443523.
[48] A. Saba, G. Chiellini, S. Frascarelli, M. Marchini, S. Ghelardoni, A. Raffaelli, M. Tonacchera, P. Vitti, T.S. Scanlan, R. Zucchi, Tissue distribution and cardiac metabolism of 3-iodothyronamine, Endocrinology 151 (2010) 5063–5073, https://doi.org/10.1210/en.2010-0491.
[49] I. Grishkovskaya, G.V. Avvakumov, G.L. Hammond, M.G. Catalano, Y.A. Muller, Steroid ligands bind human sex hormone-binding globulin in specific orientations and produce distinct changes in protein conformation, J. Biol. Chem. 277 (35) (Aug 30, 2002) 32086–32093, https://doi.org/10.1074/jbc.M203999200.
[50] A.C. Bianco, G. Anderson, D. Forrest, V.A. Galton, B. Gereben, B.W. Kim, P. A. Kopp, X.H. Liao, M.J. Obregon, R.P. Peeters, S. Refetoff, D.S. Sharlin, W. S. Simonides, R.E. Weiss, G.R. Williams, American Thyroid Association task force on approaches and strategies to investigate thyroid hormone economy and action. American Thyroid Association guide to investigating thyroid hormone economy and action in rodent and cell models, Thyroid 24 (1) (2014 Jan) 88–168, https://doi.org/10.1089/thy.2013.0109.
[51] P. Canale, G. Nicolini, L. Pitto, C. Kusmic, M. Rizzo, S. Balzan, G. Iervasi, F. Forini, Role of miR-133/Dio3 axis in the T3-dependent modulation of cardiac mitoK-ATP expression, Int. J. Mol. Sci. 23 (2022) 6549, https://doi.org/10.3390/ijms23126549.
[52] K. Itoh, T. Chiba, S. Takahashi, T. Ishii, K. Igarashi, Y. Katoh, T. Oyake, N. Hayashi, K. Satoh, I. Hatayama, M. Yamamoto, Y. Nabeshima, An Nrf2/small Maf heterodimer mediates the induction of phase II detoxifying enzyme genes through antioxidant response elements, Biochem. Biophys. Res. Commun. 236 (1997) 313–322, https://doi.org/10.1006/bbrc.1997.6943.
[53] A. Hoffmann, D. Baltimore, Circuitry of nuclear factor kappaB signaling, Immunol. Rev. 210 (2006) 171–186, https://doi.org/10.1111/j.0105-2896.2006.00375.x.
[54] G. Giannocco, M.M.L. Kizys, R.M. Maciel, J.S. de Souza, Thyroid hormone, gene expression, and central nervous system: where we are, Semin. Cell Dev. Biol. 114 (Jun 2021) 47–56, https://doi.org/10.1016/j.semcdb.2020.09.007.
[55] F.R. Jornayvaz, G.I. Shulman, Regulation of mitochondrial biogenesis, Essays Biochem. 47 (2010) 69–84, https://doi.org/10.1042/bse0470069.
[56] J.D. McGarry, N.F. Brown, The mitochondrial carnitine palmitoyltransferase system. From concept to molecular analysis, Eur. J. Biochem. 244 (1997) 1–14, https://doi.org/10.1111/j.1432-1033.1997.00001.x.
[57] B. Westermann, Mitochondrial fusion and fission in cell life and death, Nat. Rev. Mol. Cell Biol. 11 (2010) 872–884, https://doi.org/10.1038/nrm3013.
[58] W.S. Simonides, M.A. Mulcahey, E.M. Redout, A. Muller, M.J. Zuidwijk, T.J. Visser, F.W. Wassen, A. Crescenzi, W.S. da-Silva, J. Harney, F.B. Engel, M.J. Obregon, P. R. Larsen, A.C. Bianco, S.A. Huang, Hypoxia-inducible factor induces local thyroid hormone inactivation during hypoxic-ischemic disease in rats, J. Clin. Invest. 118 (2008) 975–983, https://doi.org/10.1172/JCI32824.
[59] R. Amato, E. Catalani, M. Dal Monte, M. Cammalleri, I. Di Renzo, C. Perrotta, D. Cervia, G. Casini, Autophagy-mediated neuroprotection induced by octreotide in an ex vivo model of early diabetic retinopathy, Pharmacol. Res. 128 (2018) 167–178, https://doi.org/10.1016/j.phrs.2017.09.022.
[60] B. Falkowski, A. Rogowicz-Frontczak, A. Grzelka, A. Uruska, J. Schlaffke, A. Araszkiewicz, D. Zozulinska-Ziolkiewicz, Higher free triiodothyronine concentration is associated with lower prevalence of microangiopathic complications and better metabolic control in adult euthyroid people with type 1 diabetes, Endocrine 60 (2018) 458–465, https://doi.org/10.1007/s12020-018-1582-8.

[61] V. Mehalingam, J. Sahoo, Z. Bobby, K.V. Vinod, Thyroid dysfunction in patients with type 2 diabetes mellitus and its association with diabetic complications, J. Family Med. Prim. Care 9 (2020) 4277–4281, https://doi.org/10.4103/jfmpc.jfmpc_838_20.
[62] P. Bogdanov, C. Hernández, L. Corraliza, A.R. Carvalho, R. Simó, Effect of fenofibrate on retinal neurodegeneration in an experimental model of type 2 diabetes, Acta Diabetol. 52 (2015) 113–122, https://doi.org/10.1007/s00592-014-0610-2.
[63] R. Di, Q. Luo, D. Mathew, A.D. Bhatwadekar, Diabetes alters diurnal rhythm of electroretinogram in db/db mice, Yale J. Biol. Med. 92 (2019) 155–167.
[64] J.M. Enright, S. Zhang, C. Thebeau, E. Siebert, A. Jin, V. Gadiraju, X. Zhang, S. Chen, C.F. Semenkovich, R. Rajagopal, Fenofibrate reduces the severity of neuroretinopathy in a type 2 model of diabetes without inducing peroxisome proliferator-activated receptor alpha-dependent retinal gene expression, J. Clin. Med. 10 (2020) 126, https://doi.org/10.3390/jcm10010126.
[65] J. Hanaguri, H. Yokota, M. Watanabe, S. Yamagami, A. Kushiyama, L. Kuo, T. Nagaoka, Retinal blood flow dysregulation precedes neural retinal dysfunction in type 2 diabetic mice, Sci. Rep. 11 (2021) 021–97651, https://doi.org/10.1038/s41598-021-97651-3.
[66] I.S. Samuels, B.A. Bell, A. Pereira, J. Saxon, N.S. Peachey, Early retinal pigment epithelium dysfunction is concomitant with hyperglycemia in mouse models of type 1 and type 2 diabetes, J. Neurophysiol. 113 (2015) 1085–1099, https://doi.org/10.1152/jn.00761.2014.
[67] Y. Ding, S. Yuan, X. Liu, P. Mao, C. Zhao, Q. Huang, R. Zhang, Y. Fang, Q. Song, D. Yuan, P. Xie, Y. Liu, Q. Liu, Protective effects of astragaloside IV on db/db mice with diabetic retinopathy, PLoS One 9 (2014), e112207, https://doi.org/10.1371/journal.pone.0112207.
[68] J. Li, J.J. Wang, D. Chen, R. Mott, Q. Yu, J.X. Ma, S.X. Zhang, Systemic administration of HMG-CoA reductase inhibitor protects the blood-retinal barrier and ameliorates retinal inflammation in type 2 diabetes, Exp. Eye Res. 89 (2009) 71–78, https://doi.org/10.1016/j.exer.2009.02.013.
[69] J. Li, J.J. Wang, Q. Yu, K. Chen, K. Mahadev, S.X. Zhang, Inhibition of reactive oxygen species by Lovastatin downregulates vascular endothelial growth factor expression and ameliorates blood-retinal barrier breakdown in db/db mice: role of NADPH oxidase 4, Diabetes 59 (2010) 1528–1538, https://doi.org/10.2337/db09-1057.
[70] A.K. Cheung, M.K. Fung, A.C. Lo, T.T. Lam, K.F. So, S.S. Chung, S.K. Chung, Aldose reductase deficiency prevents diabetes-induced blood-retinal barrier breakdown, apoptosis, and glial reactivation in the retina of db/db mice, Diabetes 54 (2005) 3119–3125, https://doi.org/10.2337/diabetes.54.11.3119.
[71] L. Tang, Y. Zhang, Y. Jiang, L. Willard, E. Ortiz, L. Wark, D. Medeiros, D. Lin, Dietary wolfberry ameliorates retinal structure abnormalities in db/db mice at the early stage of diabetes, Exp. Biol. Med. 236 (2011) 1051–1063, https://doi.org/10.1258/ebm.2011.010400.
[72] E. Midena, T. Segato, S. Radin, G. di Giorgio, F. Meneghini, S. Piermarocchi, A. S. Belloni, Studies on the retina of the diabetic db/db mouse. I. Endothelial cell-pericyte ratio, Ophthalmic Res. 21 (1989) 106–111, https://doi.org/10.1159/000266787.
[73] M. Wei, Y. Sun, S. Li, Y. Chen, L. Li, M. Fang, R. Shi, D. Tong, J. Chen, Y. Ma, K. Qu, M. Zhang, T. Xue, Single-cell profiling reveals Müller glia coordinate retinal intercellular communication during light/dark adaptation via thyroid hormone signaling, Protein Cell 21 (2023).
[74] A.C. Bianco, B.W. Kim, Deiodinases: implications of the local control of thyroid hormone action, J. Clin. Invest. 116 (2006) 2571–2579, https://doi.org/10.1172/JCI29812.
[75] A.C. Bianco, D. Salvatore, B. Gereben, M.J. Berry, P.R. Larsen, Biochemistry, cellular and molecular biology, and physiological roles of the iodothyronine selenodeiodinases, Endocr. Rev. 23 (2002) 38–89, https://doi.org/10.1210/edrv.23.1.0455.
[76] B. Gereben, A. Kollár, J.W. Harney, P.R. Larsen, The mRNA structure has potent regulatory effects on type 2 iodothyronine deiodinase expression, Mol. Endocrinol. 16 (7) (Jul 2002) 1667–1679, https://doi.org/10.1210/mend.16.7.0879.
[77] A. Lourbopoulos, I. Mourouzis, T. Karapanayiotides, E. Nousiopoulou, S. Chatzigeorgiou, T. Mavridis, I. Kokkinakis, O. Touloumi, T. Irinopoulou, K. Chouliaras, C. Pantos, D. Karacostas, N. Grigoriadis, Changes in thyroid hormone receptors after permanent cerebral ischemia in male rats, J. Mol. Neurosci. 54 (1) (Sep 2014) 78–91, https://doi.org/10.1007/s12031-014-0253-3.
[78] S.B. Catrina, X. Zheng, Hypoxia and hypoxia-inducible factors in diabetes and its complications, Diabetologia 64 (2021) 709–716, https://doi.org/10.1007/s00125-021-05380-z.
[79] F. Forini, G. Nicolini, L. Pitto, G. Iervasi, Novel insight into the epigenetic and post-transcriptional control of cardiac gene expression by thyroid hormone, Front. Endocrinol. 10 (2019) 601, https://doi.org/10.3389/fendo.2019.00601.
[80] A. Wulf, A. Harneit, M. Kröger, M. Kebenko, M.G. Wetzel, J.M. Weitzel, T3-mediated expression of PGC-1alpha via a far upstream located thyroid hormone response element, Mol. Cell. Endocrinol. 287 (2008) 90–95, https://doi.org/10.1016/j.mce.2008.01.017.
[81] T. Hatsukano, J. Kurisu, K. Fukumitsu, K. Fujishima, M. Kengaku, Thyroid hormone induces PGC-1α during dendritic outgrowth in mouse cerebellar Purkinje cells, Front. Cell. Neurosci. 11 (2017) 133, https://doi.org/10.3389/fncel.2017.00133.
[82] M.S. Jansen, G.A. Cook, S. Song, E.A. Park, Thyroid hormone regulates carnitine palmitoyltransferase Ialpha gene expression through elements in the promoter and first intron, J. Biol. Chem. 275 (2000) 34989–34997, https://doi.org/10.1074/jbc.M001752200.
[83] K. Hirose, A.Y. Payumo, S. Cutie, A. Hoang, H. Zhang, R. Guyot, D. Lunn, R. B. Bigley, H. Yu, J. Wang, M. Smith, E. Gillett, S.E. Muroy, T. Schmid, E. Wilson, K. A. Field, D.M. Reeder, M. Maden, M.M. Yartsev, M.J. Wolfgang, F. Grützner, T. S. Scanlan, L.I. Szweda, R. Buffenstein, G. Hu, F. Flamant, J.E. Olgin, G.N. Huang, Evidence for hormonal control of heart regenerative capacity during endothermy acquisition, Science 364 (6436) (Apr 12, 2019) 184–188, https://doi.org/10.1126/science.aar2038.
[84] R. Filadi, D. Pendin, P. Pizzo, Mitofusin 2: from functions to disease, Cell Death Dis. 9 (2018) 017–0023, https://doi.org/10.1038/s41419-017-0023-6.
[85] F. Cioffi, R. Senese, A. Lanni, F. Goglia, Thyroid hormones and mitochondria: with a brief look at derivatives and analogues, Mol. Cell. Endocrinol. 379 (2013) 51–61, https://doi.org/10.1016/j.mce.2013.06.006.
[86] D.J. Miller, M.A. Cascio, M.G. Rosca, Diabetic retinopathy: the role of mitochondria in the neural retina and microvascular disease, Antioxidants 9 (2020) 905, https://doi.org/10.3390/antiox9100905.